NATIONAL ADVISORY COMMITTEE FOR AERONAUTICS

TECHNICAL NOTE 2795

EFFECTS OF WING SWEEP ON THE UPWASH AT THE PROPELLER PLANES OF MULTIENGINE AIRPLANES

By Vernon L. Rogallo

Ames Aeronautical Laboratory
Moffett Field, Calif.

Washington
September 1952

1P

NATIONAL ADVISORY COMMITTEE FOR AERONAUTICS

TECHNICAL NOTE 2795

EFFECTS OF WING SWEEP ON THE UPWASH AT THE PROPELLER PLANES OF MULTIENGINE AIRPLANES

By Vernon L. Rogallo

SUMMARY

An analysis has been made to give a qualitative picture of the effects of wing sweep on the upwash at the propeller planes of multiengine airplanes. The method used in this analysis is, in general, the same as that given in NACA TN 2528, 1951, with the necessary extensions as suggested therein. To provide a basis for judging the effects of sweep, the method was applied to two hypothetical airplanes of the high-speed long-range type, one having an unswept wing and the other a swept-back wing. Included as a part of the report are charts which facilitate the prediction of upwash in the chord-plane region ahead of wings of various plan forms.

Comparisons of the upwash characteristics of two wings, one unswept and the other swept back 40°, indicated that the effects of wing sweep on wing upwash at the selected propeller locations were quite large. The average level of the upwash was considerably higher for the case of the swept wing. In addition to the higher level of upwash, the upwash distribution was more asymmetrical. With the wing swept, the upwash at the inboard side of a propeller disk was found to be approximately 100 percent greater than at the outboard side, whereas with the unswept wing the difference was 10 percent or less.

When considering the complete airplane, nacelle-axis inclination was found to be a powerful factor in the reduction of the over-all upflow angles at the propeller disks (the angles of local flow with respect to the nacelle axis resulting from wing upwash, upwash of bodies, and geometric angle of nacelle axis). With the nacelles inclined, it was found that the upflow angles were only slightly greater in magnitude for the airplane having the swept wing than for the airplane having the unswept wing, indicating that first-order excitation would be little greater than in the case of the airplane with the unswept wing. The asymmetry

of the upflow distribution in the case of the airplane having the swept wing was quite pronounced, particularly at the outboard nacelle location, indicating that the propellers would be subjected to higher-order excitations.

INTRODUCTION

A knowledge of the upwash angles at propeller planes is required for accurate predictions of propeller vibratory stresses. Reference 1 presents an approximate method, substantiated by comparison with experimental data, for predicting upwash at propeller planes of multiengine airplanes with unswept wings. Reference 1 also suggests a logical extension of the method to include the effects of wing sweep. In view of current interest in propeller-driven airplanes having swept-back wings and due to a total lack of experimental data concerning the upwash of such wings, it was considered valuable to apply the method of reference 1 quantitatively to shed some light on the effect of wing sweep on upwash.

In order to provide a basis for judging the effects of sweep, the method of reference 1 was applied directly to two airplanes comparable in purpose, one having an unswept wing and the other a swept-back wing. The analysis is intended to illustrate primarily the effects of sweep with no attempt to include a comprehensive survey of airplanes having swept wings.

NOTATION

A	total upflow angle, angle between the nacelle axis and the direction of the local flow[1] $(\alpha_w + \epsilon + \gamma)$, degrees
$a_{\nu n}$	coefficient dependent on wing geometry and indicating the influence of symmetric loading at span station n on the upwash angle at the span station ν
b	span of the wing measured perpendicular to the vertical plane of symmetry, feet
c	local chord of the wing,[1] feet
c_{av}	average chord[1] $\left(\frac{S}{b}\right)$, feet

[1] Measured in a plane parallel to the model vertical plane of symmetry.

c_l section lift coefficient $\left(\frac{\text{section lift}}{qc}\right)$

C_L lift coefficient $\left(\frac{\text{total lift}}{qS}\right)$

C_{L_α} lift-curve slope, per degree

$\frac{C_l c}{C_L c_{av}}$ spanwise loading coefficient

G_n dimensionless circulation $\left(\frac{\Gamma}{bV}\right)$, identical to the load coefficient $\left(\frac{C_l c}{2b}\right)$ at span station n

L body length, feet

M free-stream Mach number

n an integer defining a spanwise station on the wing quarter-chord line for which the value of circulation is defined

q free-stream dynamic pressure, pounds per square foot

S wing area, square feet

V free-stream velocity, feet per second

w induced velocity normal to the lifting surface, positive for upwash, feet per second

x fraction of propeller disk radius

y spanwise station, feet

α_w wing angle of attack,[1] degrees

β compressibility parameter $\left[\sqrt{(1-M^2)}\right]$

Γ circulation, square feet per second

γ nacelle-longitudinal-axis inclination as measured from the local chord (negative below wing-chord line), degrees

ϵ angle of upwash[1] measured from the free-stream direction, degrees

---

[1] See footnote 1, page 2.

η dimensionless lateral coordinate $\left(\frac{y}{b/2}\right)$

κ_{av} average of the ratios of the experimental section lift-curve slope to the theoretical value $\frac{2\pi}{\beta}$, all at the same Mach number

Λ sweep angle of the wing quarter-chord line, postive for sweepback, degrees

Λ_β sweep parameter which includes the effects of compressibility $\left(\tan^{-1}\frac{\tan\Lambda}{\beta}\right)$, degrees

λ wing taper ratio $\left(\frac{\text{tip chord}}{\text{root chord}}\right)$

ν an integer defining a specific point within the wing plan form for which the boundary condition of no flow through the wing is applied

τ longitudinal coordinate, distance ahead of wing quarter-chord line,[1] semispans

SCOPE

Airplane Configurations

Two hypothetical airplanes of the high-speed long-range type are used in the analysis. Since the analysis is intended to illustrate primarily the effects of wing sweep, the basic geometric parameters of the two airplane configurations have been made identical, insofar as possible, except for the wing angles of sweep and inclination of the nacelle longitudinal axis (the nacelle longitudinal axis and the propeller thrust axis are assumed coincident). The wing sweep angles are 0° and 40° as measured at the wing quarter-chord line. The principal dimensions of the airplanes, as well as the diameter and location of the propeller disks relative to the components of the airplanes, are shown in figure 1. Coordinates for the fuselage and nacelles are given in figure 2.

Flight Conditions

The flight conditions to be investigated in the analysis were chosen to give probable extremes in propeller-blade aerodynamic exciting forces.

[1] See footnote 1, page 2.

These conditions are:

1. Initial climb, flaps retracted, high gross weight, Mach number 0.33, sea-level altitude, $C_L = 0.75$

2. High speed, minimum gross weight, Mach number 0.9, 40,000-foot altitude, $C_L = 0.27$

Bases for Comparison

Comparisons of the upflow characteristics associated with the two airplane configurations will be made on the following bases:

1. Each nacelle longitudinal axis alined with the wing chord plane

2. Each nacelle longitudinal axis inclined with respect to the wing chord plane to produce equal propeller-blade aerodynamic excitation levels for high- and low-speed flight conditions

METHOD

General Procedures

The method used in this analysis is, in general, the same as that given in reference 1 with the necessary extensions as suggested therein. The upwash contribution of the fuselage and the upwash contributions of the nacelles were computed exactly as in reference 1.[2] The wing upwash contribution is computed by a prodecure differing from that given in reference 1 and hence the procedure used will be considered in detail. The summation procedure used to obtain the induced upwash of the complete airplanes is identical to the procedure given in reference 1.

Wing-Induced Upwash Angles

Span loading.- In order to determine the wing upwash angles, a knowledge of the wing span load distribution is required. It was found in the investigation reported in reference 1 that in the case of an airplane having an unswept wing the span load distribution for the wing alone could be used to calculate the upwash for the complete airplane.

[2]The resulting values of upwash for these bodies are strictly applicable only to the incompressible case. However, for the flight speeds and attitudes considered herein the effects of compressibility are negligible.

In order to check the adequacy of using such a procedure in the case of an airplane having a swept wing, the upwash was computed using available measured span load distributions for a semispan model of a 35° swept-back wing with and without a nacelle. The spanwise load distributions and the calculated upwash distributions are shown in figure 3. The large differences in the wing-alone and wing-nacelle span loadings produced a negligible change in upwash. Therefore, wing-alone span load distributions were used for the two airplane configurations of this report; the distributions were determined by the method of reference 2.

Wing upwash.- The method of reference 3 for computing wing downwash has been extended by DeYoung to enable upwash computations. The extended method (described in appendix A of this report) consists simply of the use of new $a_{\nu n}$ coefficients applicable to the region ahead of the wing in place of those given in reference 3 for the region behind the wing. The new coefficients, which are applicable to wings of various plan forms, have been computed and are given in appendix A of this report. The Prandtl-Glauert rule has been applied to account for the effects of compressibility. Although this report is not specifically directed toward providing a complete method herein, these coefficients do supply all that is needed, aside from already published work, to predict upwash in the chord-plane region ahead of a wing.

Total Upflow at Propeller Disk

Since the oscillating air load is directly dependent upon total upflow angles, A, for a given airplane flight condition (reference 4), the magnitude and distribution of the angles provide a rational basis by which to compare the severity of propeller oscillating air loads. The total upflow angle depends not only on the induced upwash of all the airplane components at the propeller plane but also on the geometric attitude of the nacelle. It is therefore necessary that the angle of zero lift and lift-curve slope for the wing-nacelle-fuselage combination be known. These data may be either estimated or obtained from model tests. For this analysis the angle of zero lift was estimated from tests of similar models. The lift-curve slopes were computed by the method given in reference 2.

Aerodynamic Exciting Parameter

It has been shown in reference 4 that propeller-blade exciting forces are a function of the product of the upflow angle and the airplane dynamic pressure of flight (i.e., the exciting parameter Aq). Since the total upflow angle includes the geometric attitude of the nacelle, the magnitude of the exciting parameter can be controlled by suitable nacelle inclination. A compromise nacelle inclination can be found so that the magnitude

of the blade exciting forces at the low-speed condition will be equal to the magnitude of the blade excitation forces at the high-speed condition. The procedure used to determine the necessary nacelle inclination is given in appendix B of this report.

RESULTS AND DISCUSSION

The results of the analysis, the examination of which is primarily directed at reaching an understanding of the likely effects of wing sweep on propeller aerodynamic excitation, will be presented in the following manner. The effects of wing sweep on wing upwash in the absence of bodies will be presented first. The total upflow angles obtained by combining the upwash contributions of the components of each airplane with the wing geometric angle of attack (nacelle axes noninclined) will then be presented. The remainder of the report will consider specific cases wherein the nacelle angles of inclination have been adjusted to give equal aerodynamic excitations at the low- and high-speed flight conditions for each airplane. The upflow characteristics for the airplanes and the upwash contributions of the components will be examined in detail.

Wing Upwash

Although the effects of compressibility have been included in all of the results, they are of small magnitude for the low-speed flight condition. Hence, the discussion of compressibility effects will be deferred to the discussion of the results on the high-speed flight condition.

Low-speed flight condition.- The spanwise distribution of upwash at constant distances ahead of the wing quarter-chord line for the swept and unswept wings is shown in figure 4. The solid lines indicate the upwash at constant values of r/β and, in the case of the swept wing, represent lines that are also swept 40°. The upwash distribution is greatly affected by wing sweep. It may be noted that, in the case of the swept wing (fig. 4(a)), the upwash drops markedly toward the wing root for constant values of r/β; whereas for the unswept wing (fig. 4(b)), the upwash increases toward the wing root. The difference in the upwash distributions of the two wings is due mainly to the difference in the sweep angles of the bound vortex.[3]

[3]As a result of sweeping the bound vortex, the left wing panel induces negative upwash ahead of the right wing panel and vice versa. This interference is most pronounced near the wing root. The greater upwash near the wing tips is due to a reduction in the interference effects of the trailing vortices.

In the case of the unswept wing, the propeller planes are parallel to the wing quarter-chord line; hence, the upwash distributions along constant values of τ/β are indicative of the wing upwash across the propeller planes. In the case of the swept wing, this correspondence does not exist because the propeller planes are not parallel to the wing chord line and therefore the value of τ/β varies across the propeller planes. The dashed lines of figure 4 indicate the wing upwash at the propeller disks.

It may be noted that in the case of the swept wing, the level of the upwash is greater at the outboard than at the inboard propeller disk; whereas in the case of the unswept wing, the level of the upwash is nearly the same at both propeller disks. This difference is due to the greater spanwise variation of upwash for the swept wing. The level of upwash is indicative of the magnitude of the first-order aerodynamic excitation. Hence, the excitation at the outboard nacelle in the case of the swept wing would be anticipated to be greater than for the case of the unswept wing. From further observation of figure 4, it may be seen that in the case of the swept wing the upwash is approximately 100 percent greater at the inboard sides of the propeller disks than at the outboard sides; whereas in the case of the unswept wing, the upwash is essentially constant. The asymmetry of the upwash is typical for swept wings and results from the fact that the values of τ/β for the inboard side of each disk are considerably less than those for the outboard side. The asymmetry of the upwash across the propeller disk is indicative of higher-order aerodynamic excitations (second-order and above). The higher-order excitations will be greater in magnitude for the case of the swept wing than for the unswept wing.

Cross plots of figure 4 have been prepared to show the upwash variation forward of the wings at constant spanwise stations. These data are presented in figure 5. The rate of change of upwash with distance ahead of the wing is nearly the same for the two wings at the inboard nacelle and not greatly different at the outboard nacelle.

High-speed flight condition.- The spanwise distributions of upwash for the two wings at the high-speed flight condition are shown in figure 6. In the case of the unswept wing, the spanwise distribution of upwash for a given value of τ/β is the same as that for the low-speed condition but is repeated here for convenience of comparison. The spanwise distributions of upwash for the two wings are greatly different. In the case of the swept wing, with the exception of the inboard portion of the wing, the upwash for a given value of τ/β is approximately 100 percent greater in magnitude than that for the unswept wing.

The dashed curves of figure 6 provide an indication of the effects of wing sweep on the upwash at the selected propeller disks. The effects of sweep on wing upwash at the propeller planes are essentially the same at the high-speed condition as those shown for the low-speed flight condition (fig. 4).

Compressibility effects on wing upwash.- Comparison of figures 4(a) (low speed) and 6(a) (high speed) indicates that, for the swept wing, there are large differences in the spanwise distributions of upwash for a, given τ/β. Since the upwash distribution is directly dependent upon the span loading and the effective wing sweep, an explanation for the differences in upwash can be obtained by investigating the effects of compressibility on these factors.

The effects of compressibility on the span loading of the wing are presented in figure 7. For the Mach numbers considered the span-loading changes are quite small for both wings. This small difference in span loading is insignificant in terms of upwash.

Since the effects of compressibility on the span loadings were negligible, the dissimilarity in the upwash of figures 4(a) and 6(a) must result from changes in the effective sweep angle. As the Mach number is increased from 0.33 to 0.90, the effective sweep angle of the wing, Λ_β, changes from 41-1/2° to 62-1/2°. In the case of the unswept wing, there is no difference in the upwash distribution for a given value of τ/β for the low- and high-speed conditions since the sweep parameter Λ_β is equal to zero for both flight conditions.

The effects of compressibility on the upwash across the selected propeller disks are shown in figure 8. It may be noted that the upwash for a given lift coefficient has been considerably reduced at the high-speed condition. The reduction in upwash at the propeller disks with increase in Mach number results from the increased values of τ/β, shown in figure 9. However, in the case of the swept wing, the large increase in upwash for given values of τ/β (see figs. 4(a) and 6(a)) offsets to some extent the effects of increasing τ/β.

The variation in the upwash as a function of Mach number is shown in figure 10 for a specific geometric location ahead of the respective wing quarter-chord lines. The magnitude of the upwash is shown to be greater for the swept wing. The rate of change of the upwash with Mach number is not greatly different for the two wings.

Total Upflow for the Airplanes

Nacelles noninclined.- The total upflow angles for the two airplane configurations are shown in figure 11 for both low- and high-speed flight conditions with the nacelles noninclined with respect to the local wing-chord line. The upflow angles for the configuration having the swept wing are greater for all cases. Noticeable asymmetry across the propeller disk, particularly for the low-speed case, is shown for the swept wing, the upflow angles being greater at the inboard side of the nacelles. In the case of the unswept wing the upwash angles on diametrically opposite sides of the propeller disk are more nearly equal.

The total upflow angle includes the geometric angle of attack of the wings; hence, part of the difference in the level of the upflow angles shown for the two airplanes can be attributed to a difference in the lift-curve slope. Figure 12 shows the lift-curve slopes for the two wings as functions of Mach number. The lift-curve slope is greater for the unswept wing by approximately 27 percent for the low-speed condition and 63 percent for the high-speed condition. Hence, for the same lift coefficient the swept-wing airplane wing angle of attack is higher and the difference in wing angles of attack between the low-speed and high-speed conditions is greater than for the airplane with the unswept wing.

Nacelles inclined.- Figure 13 shows the total upflow angles and the required nacelle inclinations for the case of nearly equal aerodynamic excitation at low and high speeds. As a result of inclining the nacelles, the upflow angles for the low-speed case have been reduced by approximately 50 percent for both airplanes. It may be noted that the absolute values of the upflow angles for the high-speed case are greater in magnitude than when the nacelles were uninclined. Comparison of the upflow angles for the two airplanes shows the configuration having the swept wing to have somewhat greater upflow angles. The asymmetry across the propeller disks is characteristic of the swept-wing case and, as is evident from figure 13, is most pronounced at low speed. It is of interest to note that the nacelles on the configuration having the swept wing required more inclination than those of the unswept-wing case.

Upwash Contribution of the Airplane Components, Nacelles Inclined

The component parts of the total upwash angles as well as the total upwash angles for the airplanes with nacelles inclined are shown in figures 14 and 15 for the low- and high-speed flight conditions. Only the case of the airplanes with inclined nacelles is considered since it is felt that this provides a more rational basis by which to compare the two airplanes.

It may be noted in figures 14(a) and 14(b) that for both airplanes the wing contributes the principal part of the upwash at the low-speed condition. The wing upwash is higher for the case of the swept-wing airplane, particularly at the outboard propeller plane. The fuselage contribution for the case of the swept-wing airplane is approximately 50 percent greater than that for the case of the unswept-wing airplane. This difference is due to a greater effective angle of attack of the fuselage of the swept-wing airplane, resulting from a greater geometric angle of attack and greater wing-induced upwash. It may also be noted in figure 14(a) that in the case of the swept-wing airplane the inboard nacelle contributes upwash at the outboard propeller plane, whereas for the case of the unswept-wing airplane (fig. 14(b) such inboard nacelle

effects are negligible. The upwash contributions of the inboard and outboard nacelles at their respective propeller disks are nearly equal in magnitude for both airplanes.

The summation of the upwash induced by the components is shown in figures 14(a) and 14(b) for the two airplanes at the low-speed flight condition. The interference effects of the bodies contribute to the asymmetry of the upwash across the propeller disks, in particular at the inboard propeller location of the swept-wing airplane (fig. 14(a)). A comparison of the total upwash angles, ϵ, of figure 14 with the total upflow angles, A, of figure 13 indicates the upwash to be a high percentage of the total upflow.

In the case of the high-speed flight condition (fig. 15), the upwash contributions of the components are considerably reduced from those shown for the low-speed flight condition (fig. 13). The fuselage contribution of upwash has become nil for the swept-wing case and is of little significance in the case of the unswept wing. The average level of the wing upwash is greater in the case of the swept wing than that for the case of the unswept wing. As a result of nacelle inclination the nacelle effective angle of attack is negative in sense and hence the nacelle produces negative upwash.

Comparison of the total upwash angles, ϵ, of figure 15 with the total upflow angles, A, of figure 13 indicates the geometric angle of attack of the nacelle to be the predominant factor in the upflow angle at the high-speed flight condition.

Aerodynamic Exciting Parameter, Nacelles Inclined

Figure 16 shows the values of the aerodynamic exciting parameter Aq, which are indicative of the oscillating air loads. Note that for a given nacelle and airplane configuration the average values of the aerodynamic exciting factor, Aq, are very nearly equal in absolute magnitude for the high- and low-speed flight conditions. This balance in the exciting parameter was the requirement previously made in order to determine the nacelle angle of inclination. The principal effect of wing sweep is to increase the aerodynamic excitation at the inboard side of the propeller disk at the low-speed condition. For the case of the swept-wing airplane, the greater magnitudes of the exciting parameter shown for both flight conditions indicate that the first-order excitation will be greater than for the case of the unswept-wing airplane. The asymmetry of the distribution of the exciting parameter indicates the possibility of increased magnitudes of the higher-order components of the oscillating air load.

CONCLUDING REMARKS

Comparisons of the upwash characteristics of the unswept and the 40° swept-back wings indicated that the effects of wing sweep on the spanwise distribution of upwash were appreciable. The magnitude of the upwash in the case of the swept wing was shown to decrease toward the wing root for constant values of r/β while, in contrast, in the case of the unswept wing the upwash decreased toward the wing tip. The average level of the upwash for constant values of r/β was higher for the case of the swept wing.

Comparisons of the upwash characteristics of the two wings at the selected propeller planes indicated that the effects of wing sweep on wing upwash in these regions were quite large. The average level of the upwash was considerably higher for the case of the outboard nacelle of the swept wing. In addition to the higher level of upwash, the upwash distribution was more asymmetrical. With the wing swept, the upwash at the inboard side of a propeller disk was found to be approximately 100 percent greater than at the outboard side; whereas, with the unswept wing, the difference was 10 percent or less.

When considering the complete airplane, nacelle-axis inclination was found to be a powerful factor in the reduction of the over-all upflow angles at the propeller disks (the angles of local flow with respect to the nacelle axis resulting from wing upwash, upwash of bodies, and geometric angle of nacelle axis). With the nacelles inclined, it was found that the upflow angles were only slightly greater in magnitude for the airplane having the swept wing than for the airplane having the unswept wing, indicating that first-order excitation would be little greater than in the case of the airplane with the unswept wing. The asymmetry of the upflow distribution in the case of the airplane having the swept wing was quite pronounced indicating that the propellers would be subjected to higher-order excitations.

Ames Aeronautical Laboratory
National Advisory Committee for Aeronautics
Moffett Field, Calif., July 17, 1952

APPENDIX A

PREDICTION OF UPWASH OF ARBITRARY WINGS

Reference 3 indicates that if the symmetrical loading distribution is known, from computations or measurements, the values of the $a_{\nu n}$ coefficients given in reference 3 can be used to find corresponding values of the downwash. The same basic equations given in reference 3 are applicable to the computation of upwash, but new values of the $a_{\nu n}$ coefficients must be used.

The upwash can be found at specific points in the chord-plane region between the wing tips and ahead of the wing leading edge. The general expression for the upwash is given as

$$\left(\frac{w}{V}\right)_{\tau/\beta,\eta_\nu} = \sum_{n=1}^{4} a_{\nu n} G_n$$

where the $a_{\nu n}$ coefficients are obtained from figure 17. The specific station at which the upwash may be found corresponds to $\nu = 1, 2, 3, 4,$ or $\eta_\nu = \cos(\nu\pi/8) = 0.924, 0.707, 0.383,$ and 0, respectively. For convenience, the preceding equation is rewritten so that the upwash angle and loading distribution are in terms of unit lift coefficient. Thus,

$$\left(\frac{w/V}{\beta C_L/\kappa_{av}}\right)_{\tau/\beta,\eta_\nu} = \frac{1}{2\left[\frac{\beta(b^2/S)}{\kappa_{av}}\right]} \sum_{n=1}^{4} a_{\nu n}\left(\frac{C_l c}{C_L c_{av}}\right)_n$$

where the quantity b^2/S is the wing aspect ratio and $C_l c/C_L c_{av}$ is the span loading coefficient. Both $a_{\nu n}$ and $C_l c/C_L c_{av}$ are affected by compressibility, since they have been determined as functions of the parameters $\frac{\beta(b^2/S)}{\kappa_{av}}$ and Λ_β.

APPENDIX B

METHOD FOR COMPUTING NACELLE-AXIS INCLINATION FOR MINIMUM AERODYNAMIC EXCITING LEVELS

There exists a nacelle inclination such that the magnitude of the blade exciting forces at the low-speed condition will be equal to the magnitude of the blade excitation forces at the high-speed condition. This relation may be analytically expressed by use of the aerodynamic exciting parameter as

$$A_L q_L = -A_H q_H \tag{B1}$$

where

$A_L q_L$ exciting parameter at low speed

$A_H q_H$ exciting parameter at high speed

The upflow angles at the horizontal center line of a given propeller disk are usually not equal at all radii, and hence expression (B1) may not be satisfied at all blade elements. However, since the aerodynamic loading is a maximum over the outer portion of a blade and since the loading in this region is most important in terms of the aerodynamic bending moment, an average value of the upwash at diametrically opposite sides of the disk in the vicinity of the 0.7 radius station is used to satisfy expression (B1).

The total upflow angle A as measured at the horizontal center line of the propeller disk may be expressed as

$$A = \alpha_w + \left(\epsilon_w + \epsilon_n + \epsilon_b\right) + \gamma \tag{B2}$$

where

α_w geometric angle of attack of the wing

ϵ_w wing-induced upwash at α_w

ϵ_n nacelle-induced upwash

ϵ_b upwash of adjacent body

γ geometric angle of nacelle axis relative to wing chord

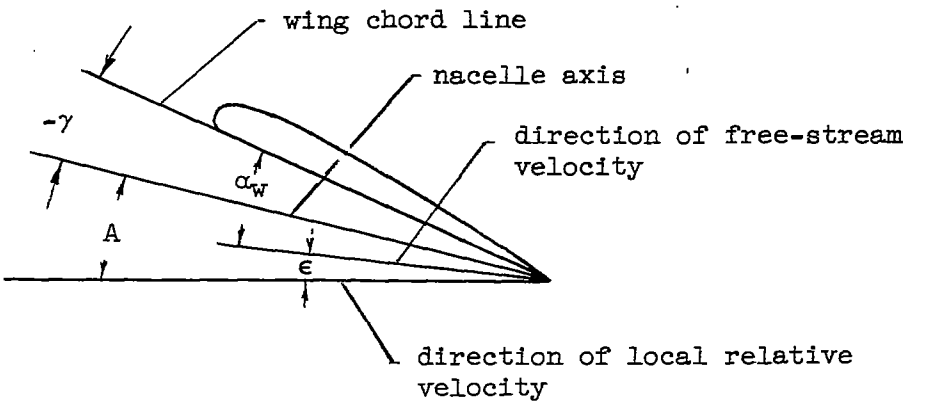

By substituting the appropriate expressions for A_L and A_H in equation (B1)

$$\left[\alpha_{w_L} + \bar{\epsilon}_{w_L} + \left(\frac{\epsilon}{\alpha}\right)_n \left(\gamma + \varphi_L\right) + \bar{\epsilon}_{b_L} + \gamma\right] q_L =$$

$$-\left[\alpha_{w_H} + \bar{\epsilon}_{w_H} + \left(\frac{\epsilon}{\alpha}\right)_n \left(\gamma + \varphi_H\right) + \bar{\epsilon}_{b_H} + \gamma\right] q_H \qquad \text{(B3)}$$

where the bar denotes the average of the upwash angles at the 0.7 radius station on diametrically opposite sides of the disk, φ represents the upwash at the propeller disk center which is equal to $(\alpha_w+\epsilon_w+\epsilon_b)$, and $(\epsilon/\alpha)_n$ represents the nacelle-upwash constant at the 0.7 radius station obtained from reference 1. Collecting terms and solving for γ, the expression may be written as

$$\gamma = -\left\{\frac{\left[\alpha_{w_L} + \bar{\epsilon}_{w_L} + \bar{\epsilon}_{b_L} + \left(\frac{\epsilon}{\alpha}\right)_n \varphi_L\right] q_L + \left[\alpha_{w_H} + \bar{\epsilon}_{w_H} + \bar{\epsilon}_{b_H} + \left(\frac{\epsilon}{\alpha}\right)_n \varphi_H\right] q_H}{\left(q_H + q_L\right)\left[1 + \left(\frac{\epsilon}{\alpha}\right)_n\right]}\right\} \qquad \text{(B4)}$$

Thus the nacelle axis inclination is found.

REFERENCES

1. Yaggy, Paul F.: A Method for Predicting the Upwash Angles Induced at the Propeller Plane of a Combination of Bodies With an Unswept Wing. NACA TN 2528, 1951.

2. DeYoung, John, and Harper, Charles W.: Theoretical Symmetric Span Loading at Subsonic Speeds for Wings Having Arbitrary Plan Form. NACA Rep. 921, 1948.

3. DeYoung, John: Theoretical Symmetric Span Loading due to Flap Deflection for Wings of Arbitrary Plan Form at Subsonic Speeds. NACA TN 2278, 1951.

4. Vogeley, A. W.: Calculation of the Effect of Thrust-Axis Inclination on Propeller Disk Loading and Comparison with Flight Measurements. NACA TN 1721, 1948.

Note: All dimensions are in feet.

Wing area	2,000.0 ft^2
Span	141.4 ft
Aspect ratio	10.0
Taper ratio	0.4
Sweep of 1/4 chord	40.0° or 0°
Incidence	3.0°
Propeller diameter	14.0 ft

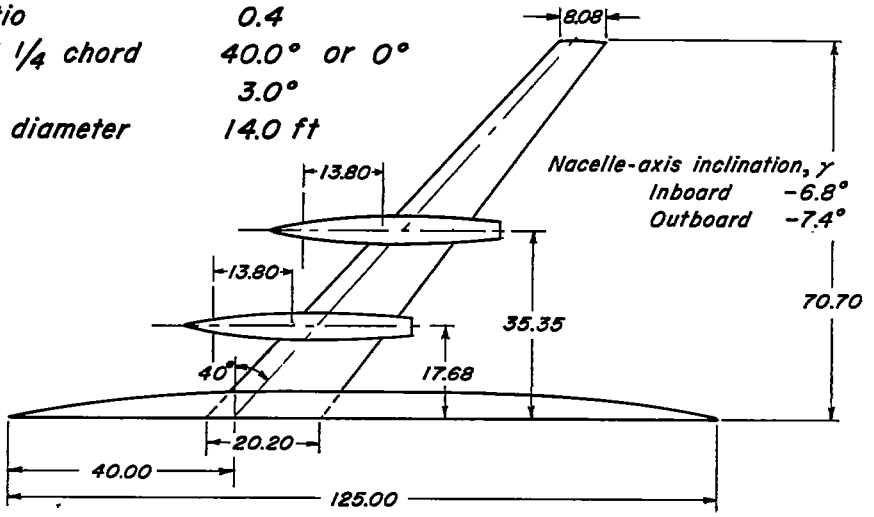

(a) Configuration with swept-back wing.

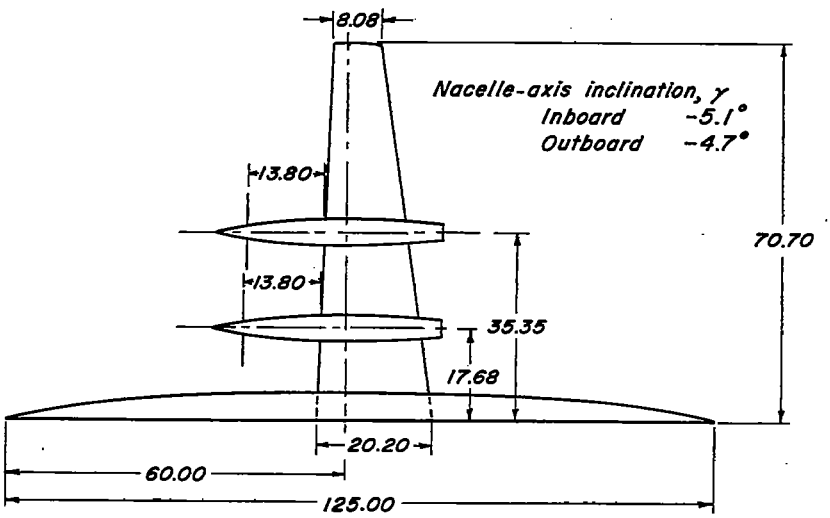

(b) Configuration with unswept wing.

Figure 1.- Geometric characteristics of the two airplane configurations analyzed.

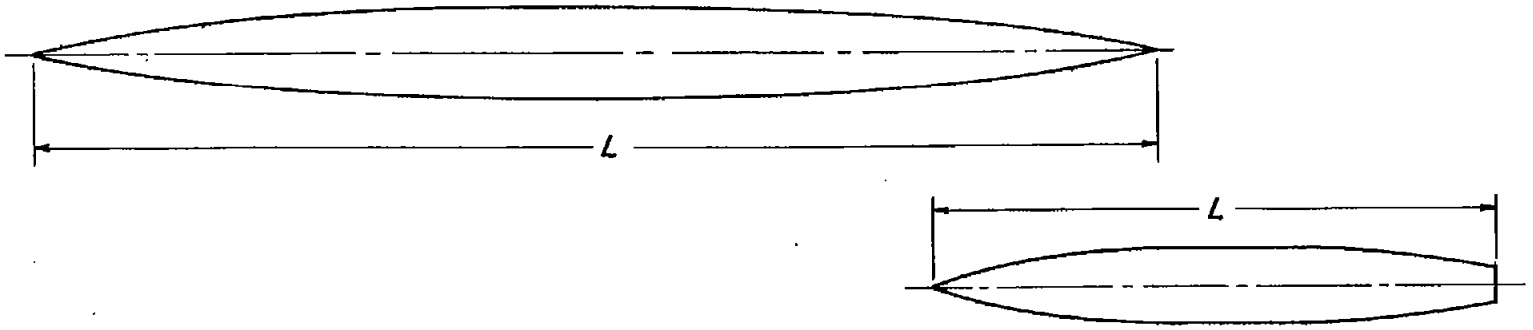

Fuselage Coordinates	
Sta % L	Rad % L
0	0
0.625	0.264
1.250	.420
2.500	.700
5.000	1.152
7.500	1.536
10.000	1.860
15.000	2.414
20.000	2.864
25.000	3.224
30.000	3.512
35.000	3.727
40.000	3.879
45.000	3.970
50.000	4.000
L = 125 feet	

Nacelle Coordinates			
Sta % L	Rad % L	Sta % L	Rad % L
0	0	40.00	6.21
1.25	0.65	44.58	6.24
2.50	1.16	50.00	6.24
5.00	2.00	60.00	6.24
7.50	2.71	68.78	6.24
10.00	3.25	75.00	6.12
15.00	4.22	80.00	5.60
20.00	4.96	85.00	5.27
25.00	5.50	90.00	4.10
30.00	5.85	95.00	3.86
35.00	6.07	100.00	2.98
L = 40 feet			

NACA

Figure 2.- Geometric characteristics of the fuselage and nacelle.

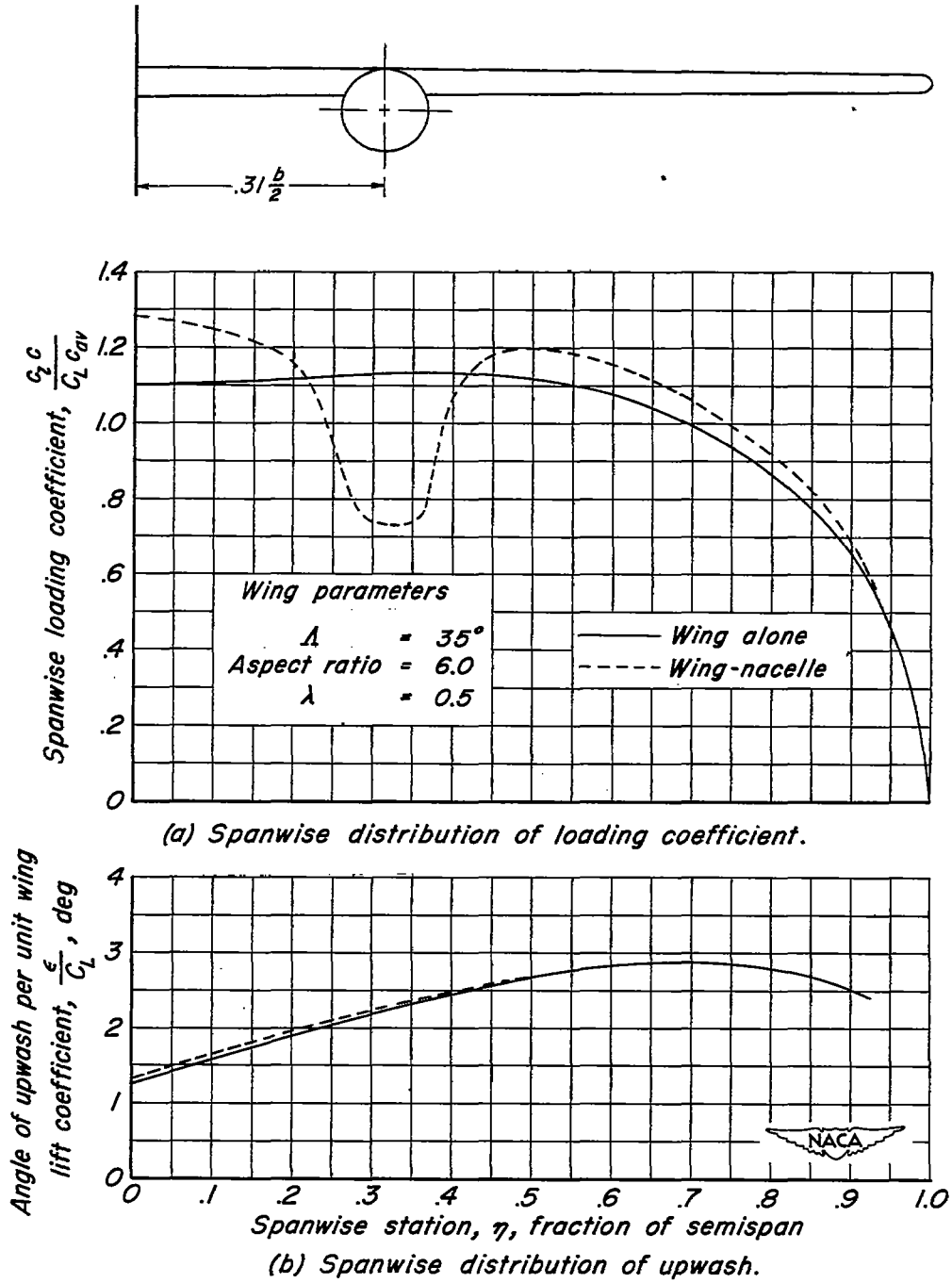

Figure 3.— Comparisons of measured spanwise load distributions for a wing alone and wing-nacelle combination and the resultant computed upwash distributions at a distance of one chord ahead of the wing leading edge. Mach number, 0.18 ; lift coefficient, 0.32.

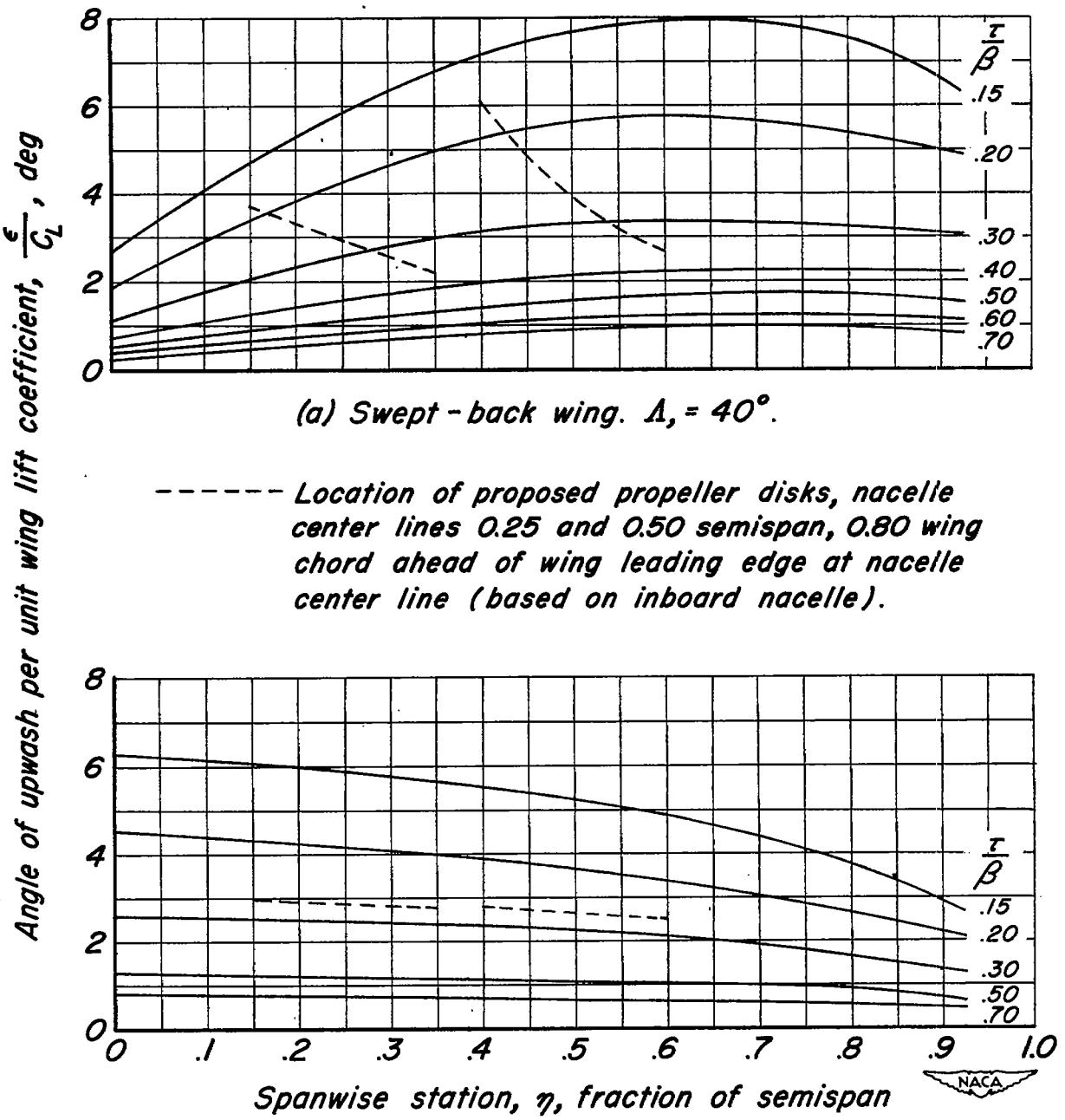

(a) Swept-back wing. $\Lambda_{.25} = 40°$.

------ Location of proposed propeller disks, nacelle center lines 0.25 and 0.50 semispan, 0.80 wing chord ahead of wing leading edge at nacelle center line (based on inboard nacelle).

(b) Unswept wing.

Figure 4.– The spanwise distribution of upwash at constant distances ahead of the wing quarter-chord line for an unswept and a swept-back wing. Mach number, 0.33.

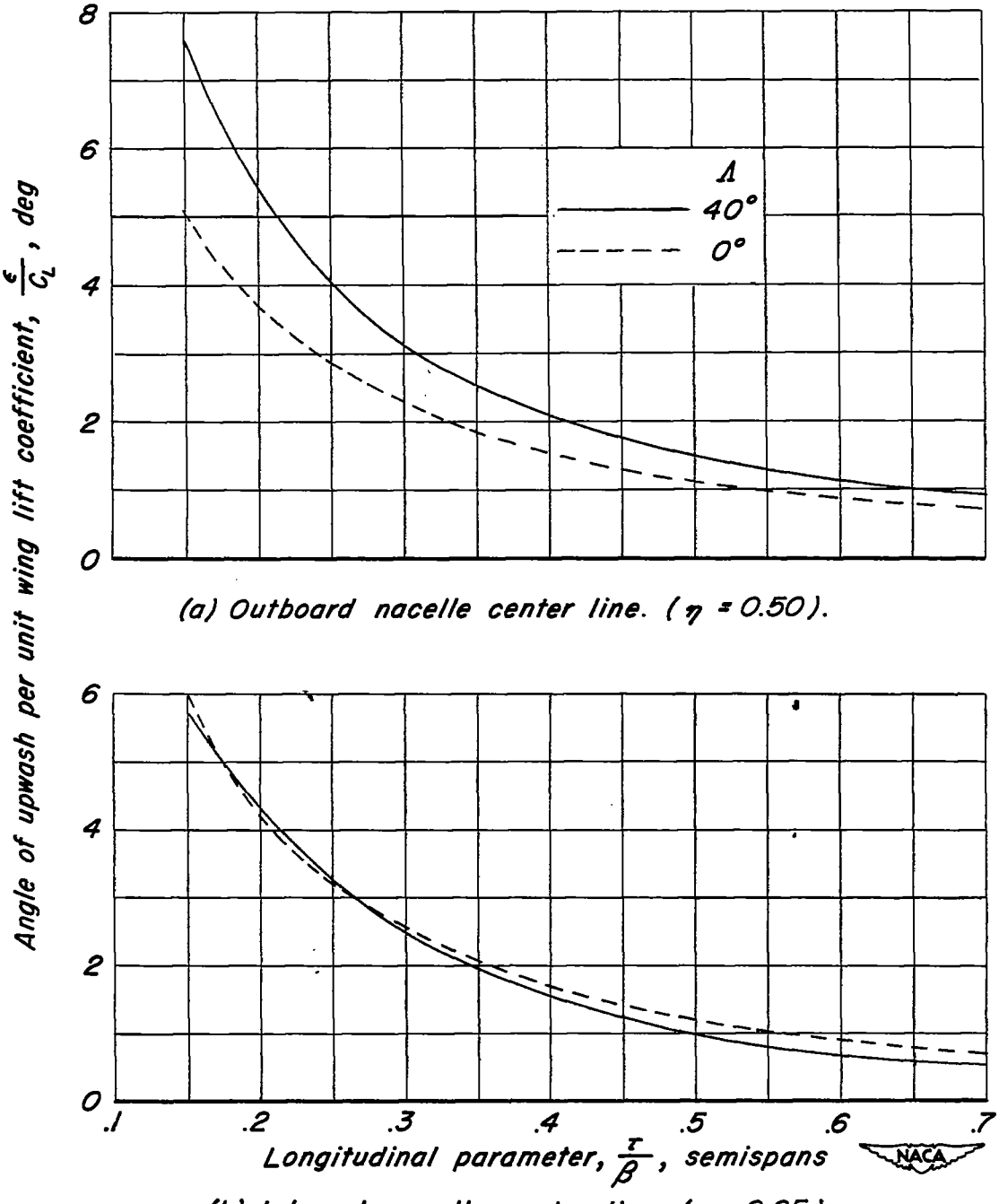

(a) Outboard nacelle center line. (η = 0.50).

(b) Inboard nacelle center line. (η = 0.25).

Figure 5.—The variation of upwash as a function of distance ahead of the wing quarter-chord line measured in a streamwise direction. Mach number, 0.33 .

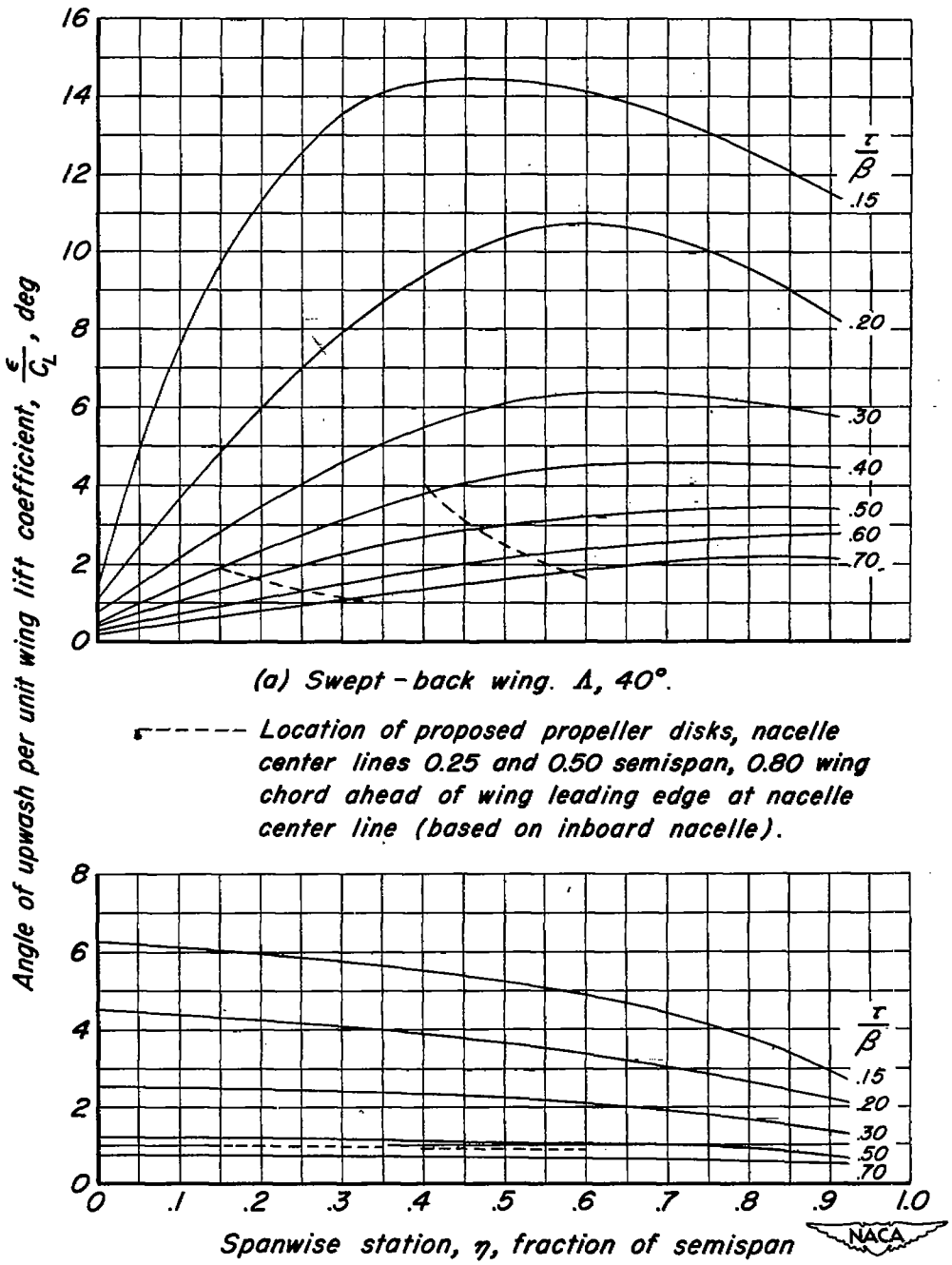

Figure 6.–The spanwise distribution of upwash at constant distances ahead of the wing quarter-chord line for an unswept and a swept-back wing. Mach number, 0.90.

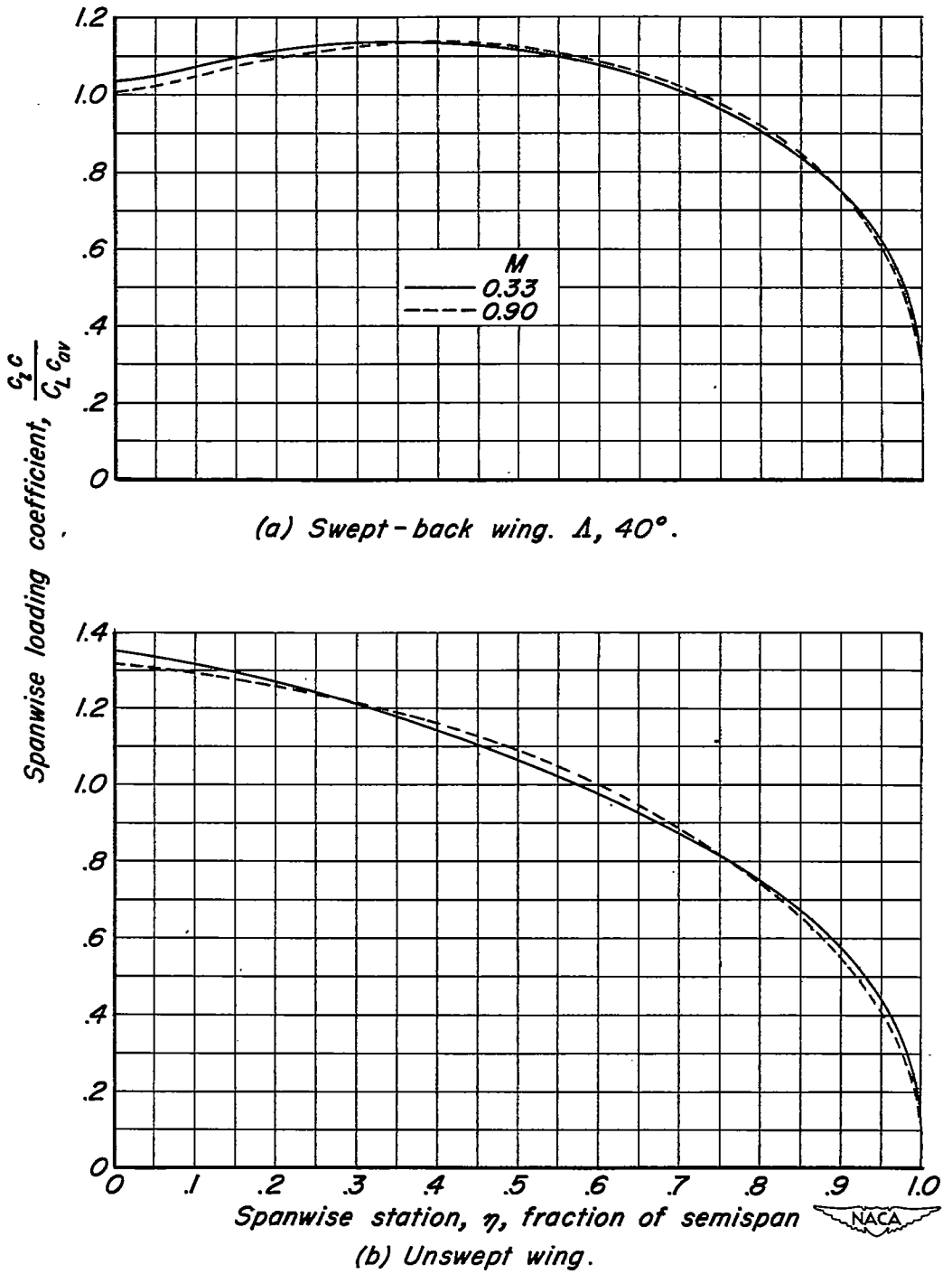

(a) Swept-back wing. Λ, 40°.

(b) Unswept wing.

Figure 7.- A comparison of the effect of Mach number on the spanwise loading coefficient for an unswept and a swept-back wing.

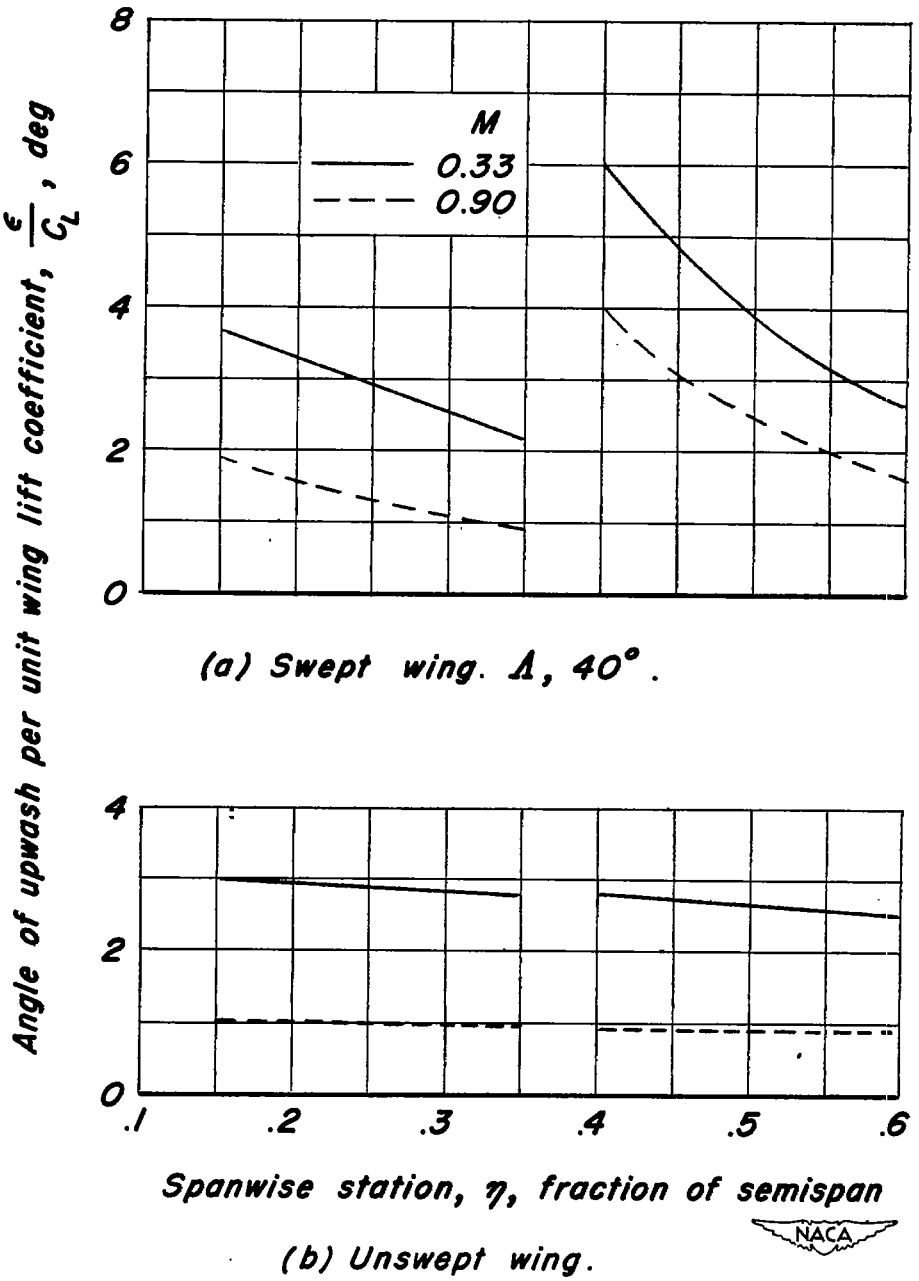

Figure 8.– The effect of compressibility on the distribution of upwash at the selected propeller disks.

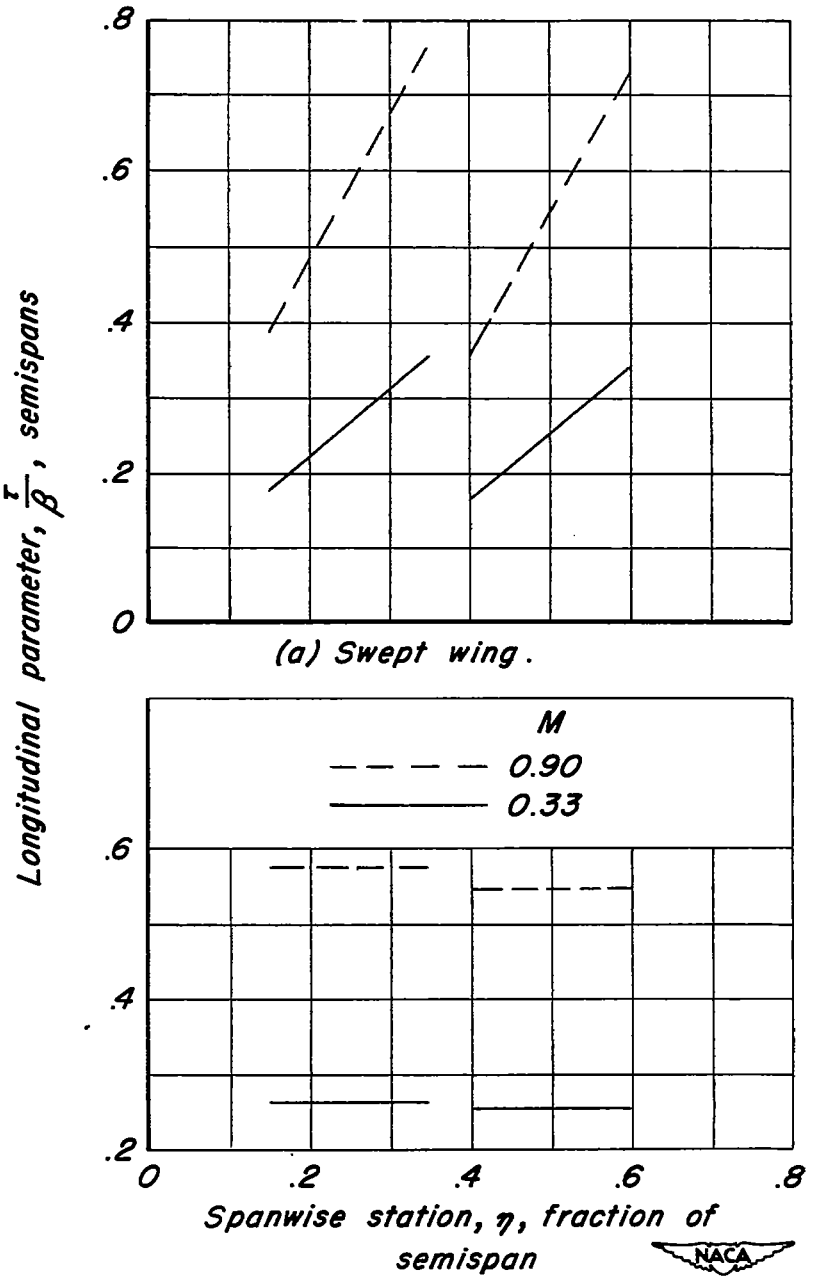

Figure 9.- The effect of compressibility on the longitudinal parameter, τ/β, at the selected propeller disks for the low and high-speed flight conditions.

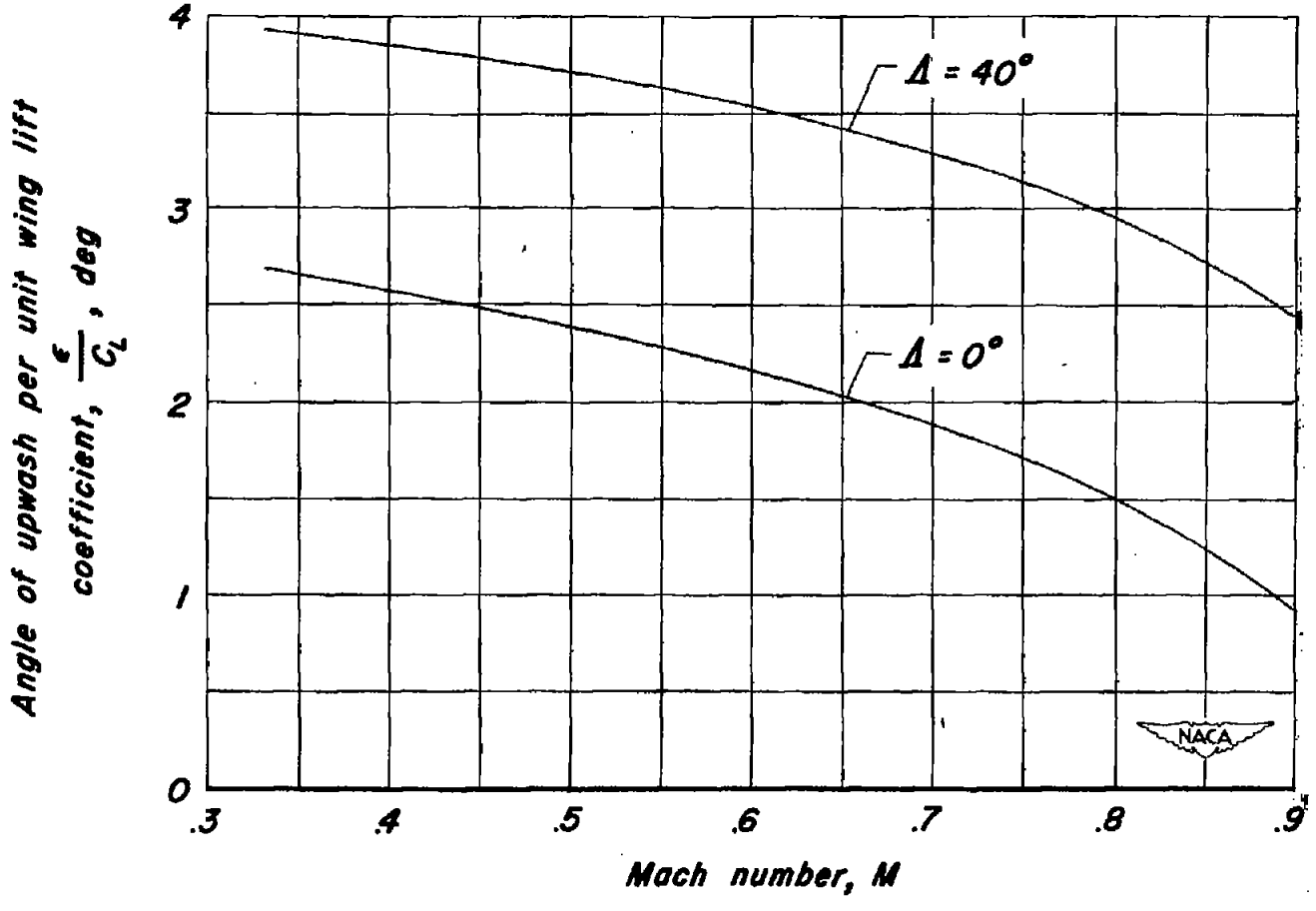

Figure 10.– A comparison of the effects of Mach number on the wing-induced upwash at a point located 0.8 wing chord ahead of the wing leading edge at the 0.50 semispan station for an unswept and a swept-back wing.

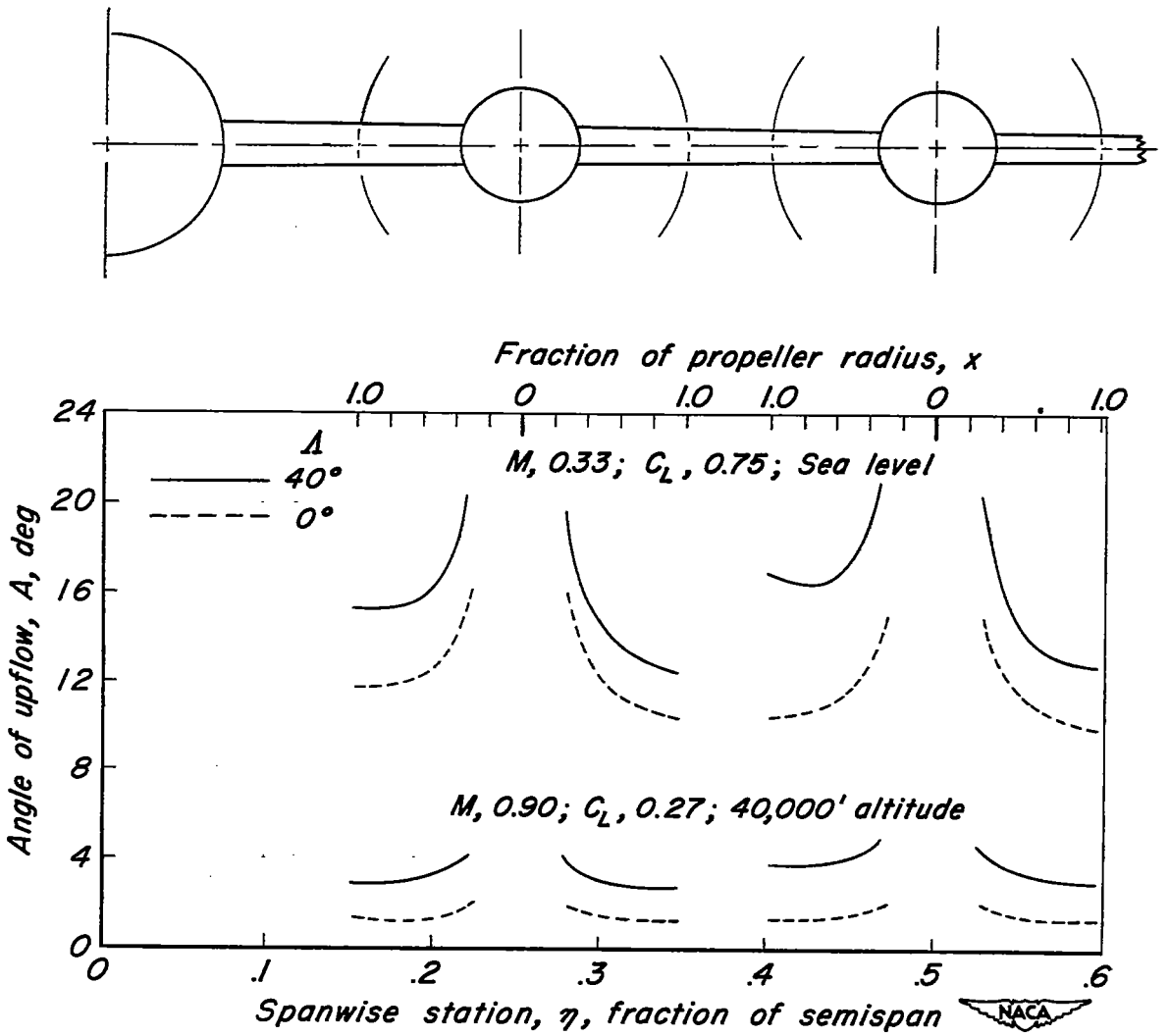

Figure 11.—The distribution of the total upflow angle at the horizontal center lines of the propeller disks of the two hypothetical airplanes. Nacelle-axis inclination, (γ), 0°.

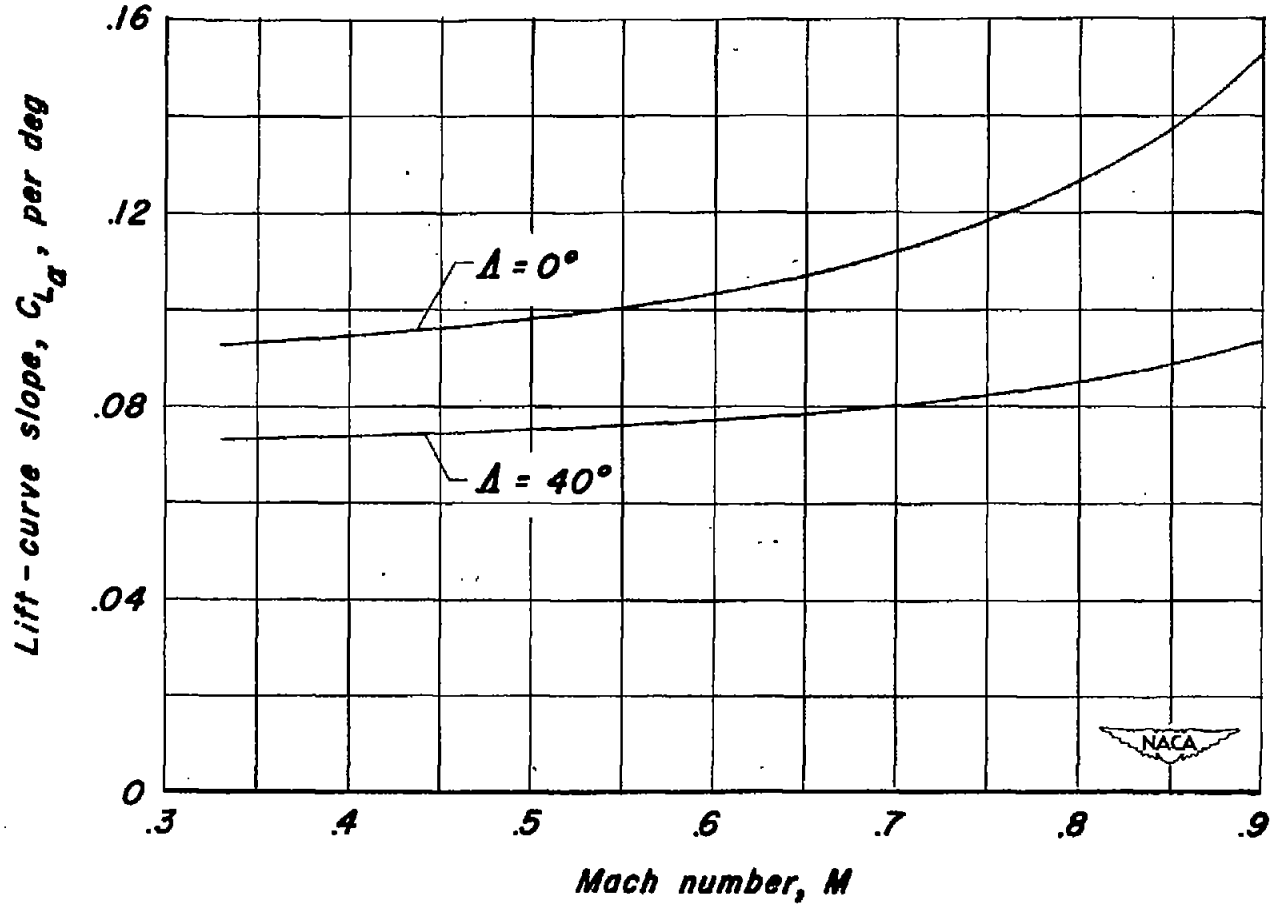

Figure 12.- Comparison of the effects of Mach number on wing lift-curve slope for an unswept and a swept-back wing.

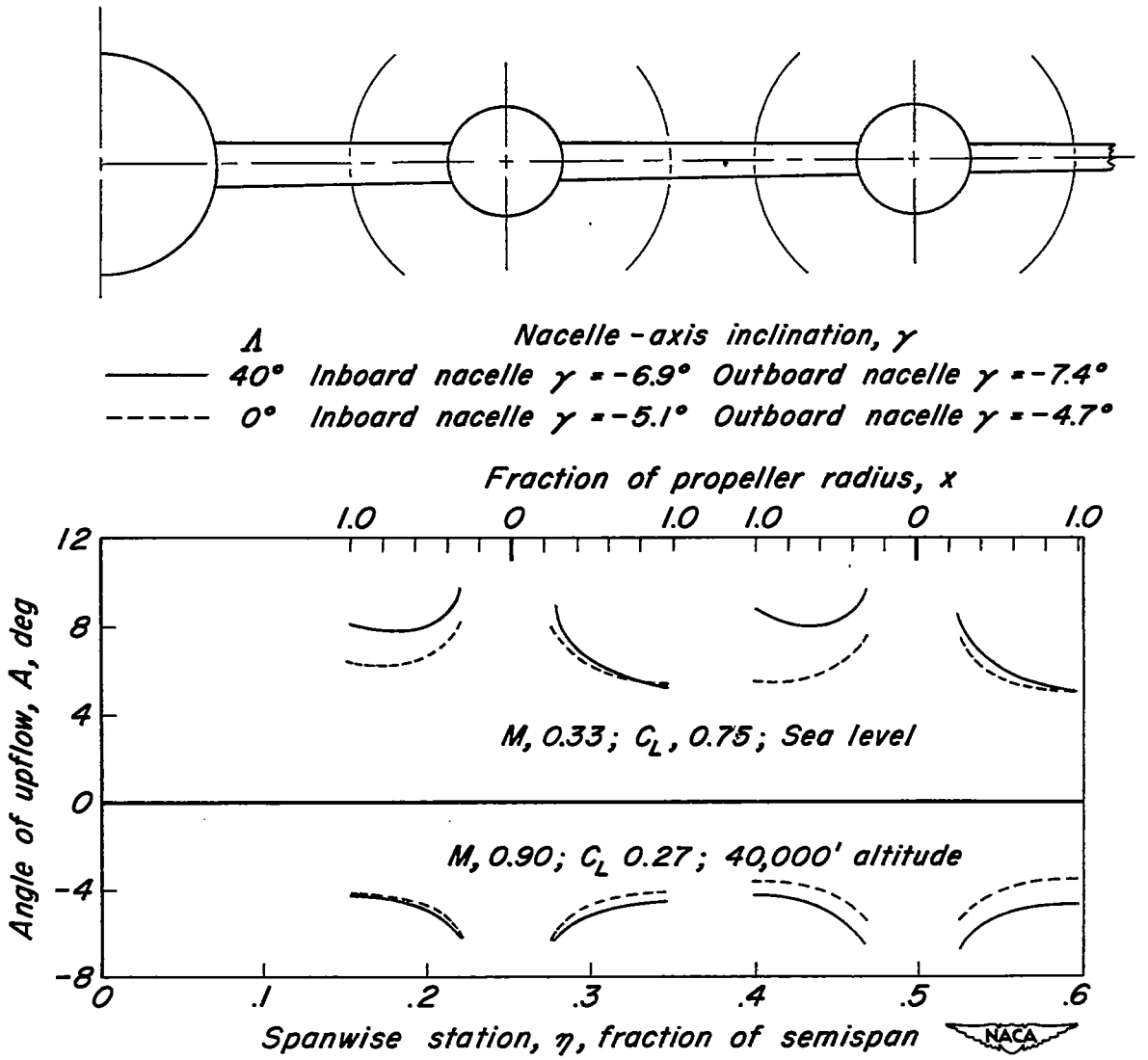

Figure 13.—The distribution of the total upflow angle at the horizontal center lines of the propeller disks of the two hypothetical airplanes with the nacelles inclined.

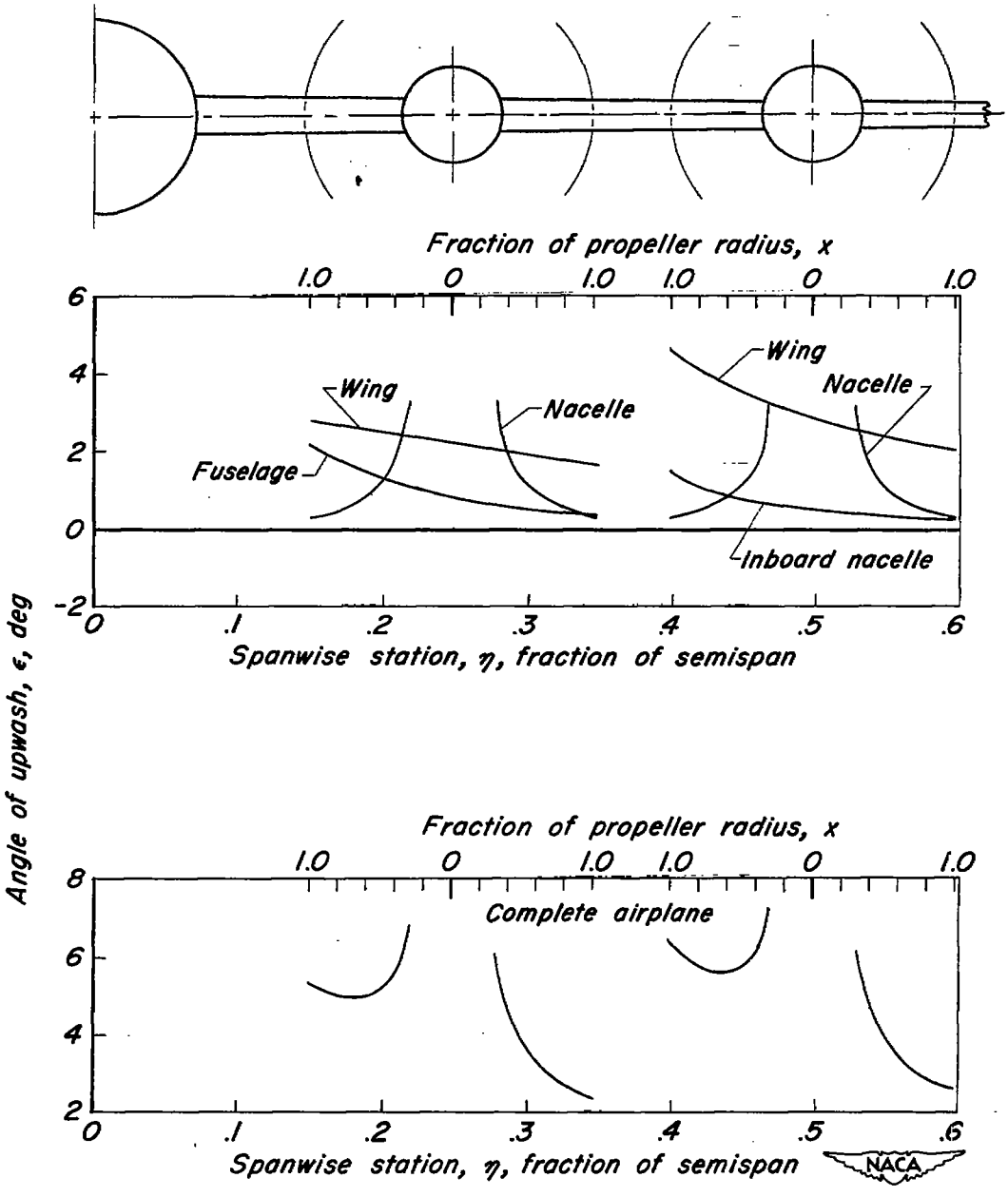

(a) Λ, 40°; a_w, 9.7°; $\gamma_{In'bd}$, -6.9°; $\gamma_{Out'bd}$, -7.4°

Figure 14.–The distribution of the angle of upwash at the horizontal center lines of the propeller disks of the two hypothetical airplanes. Mach number, 0.33; lift coefficient, 0.75; altitude, sea level.

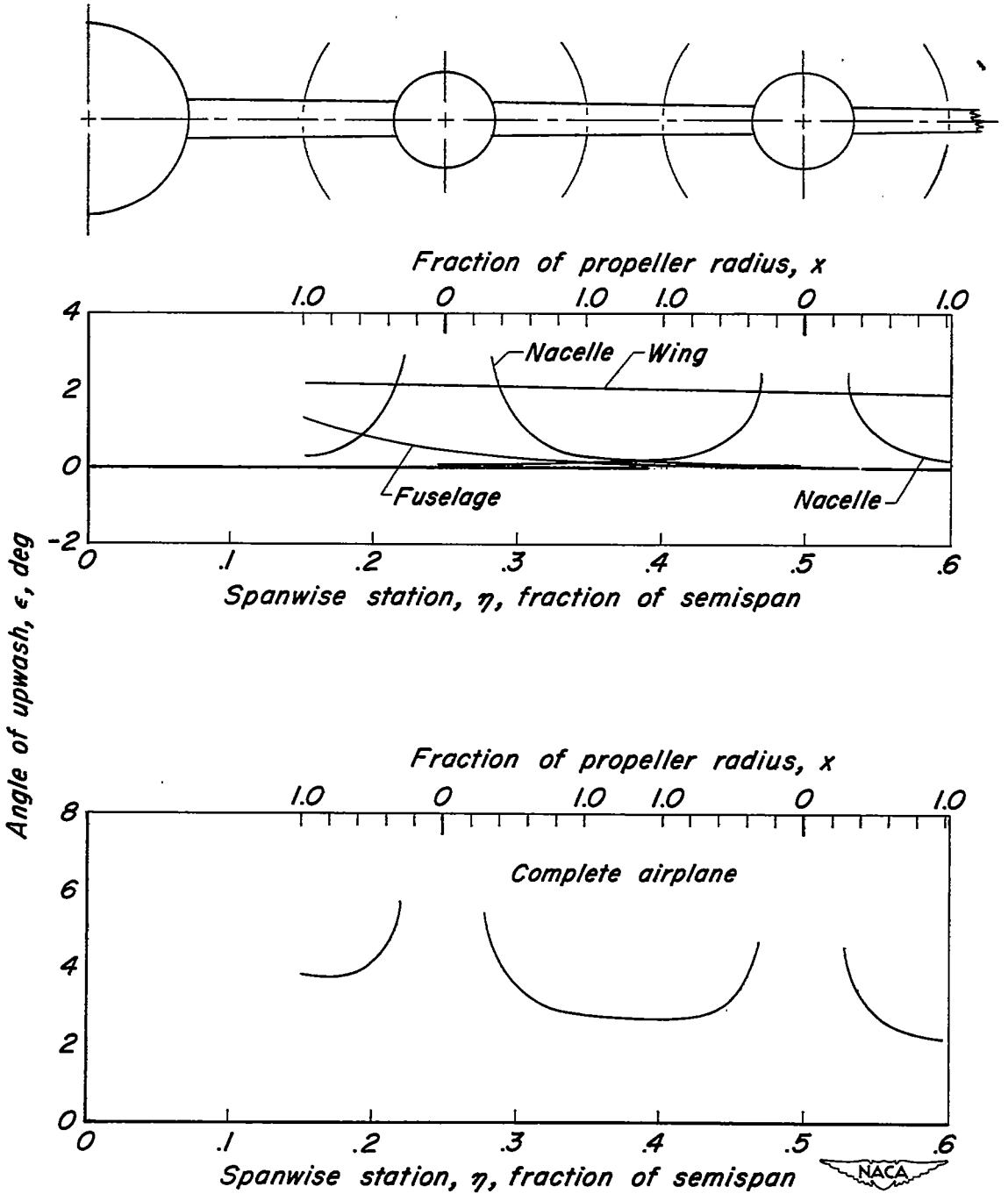

(b) Λ, 0°; a_w, 7.6°; $\gamma_{in'bd}$, -5.1°; $\gamma_{out'bd}$ -4.7°

Figure 14.- Concluded.

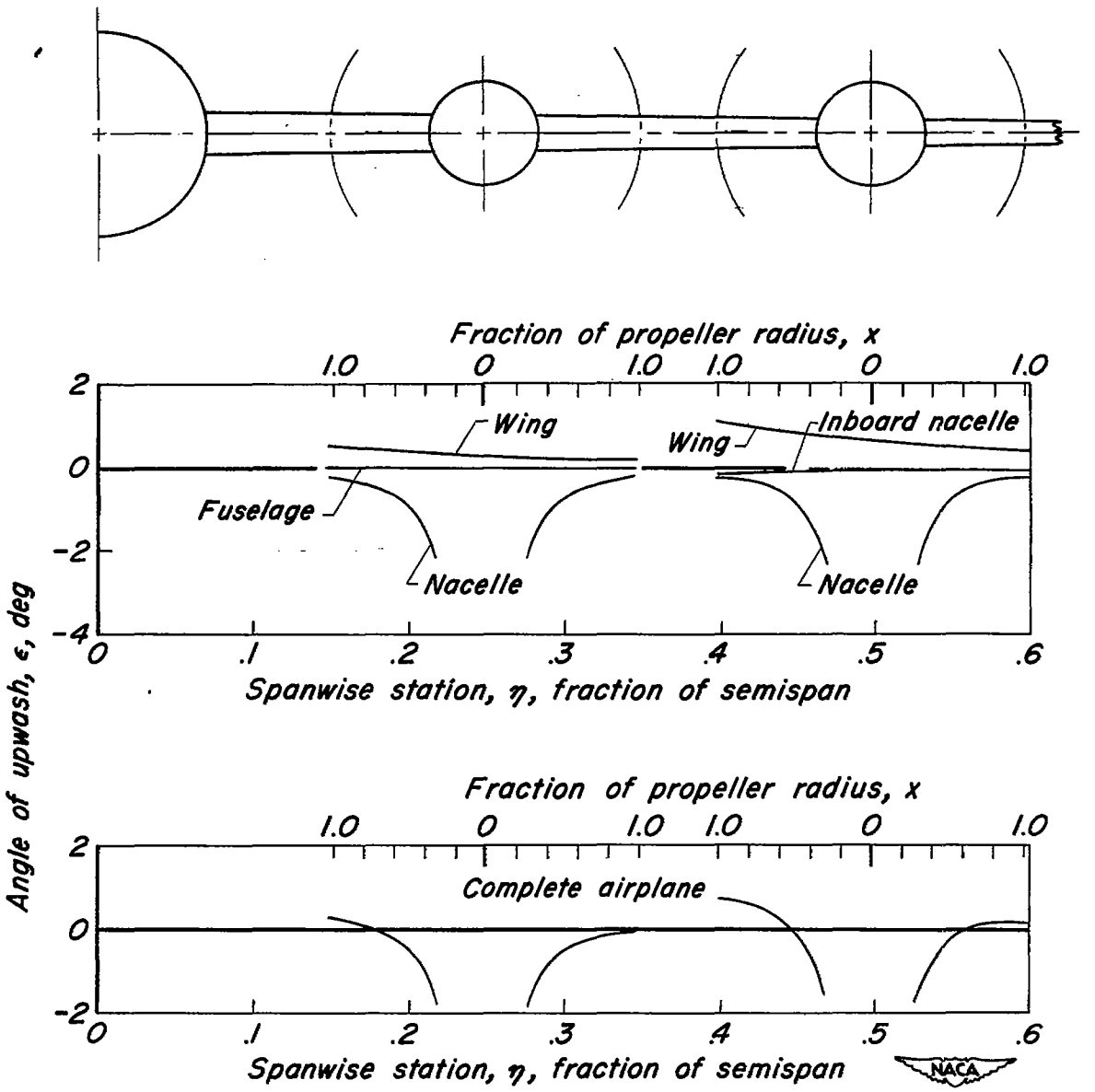

(a) Λ, 40°; a_w, 2.4°; $\gamma_{In'bd}$, -6.9°; $\gamma_{Out'bd}$, -7.4°

Figure 15.- The distribution of the angle of upwash at the horizontal center lines of the propeller disks of the two hypothetical airplanes. Mach number, 0.90; lift coefficient, 0.27; altitude, 40,000 feet.

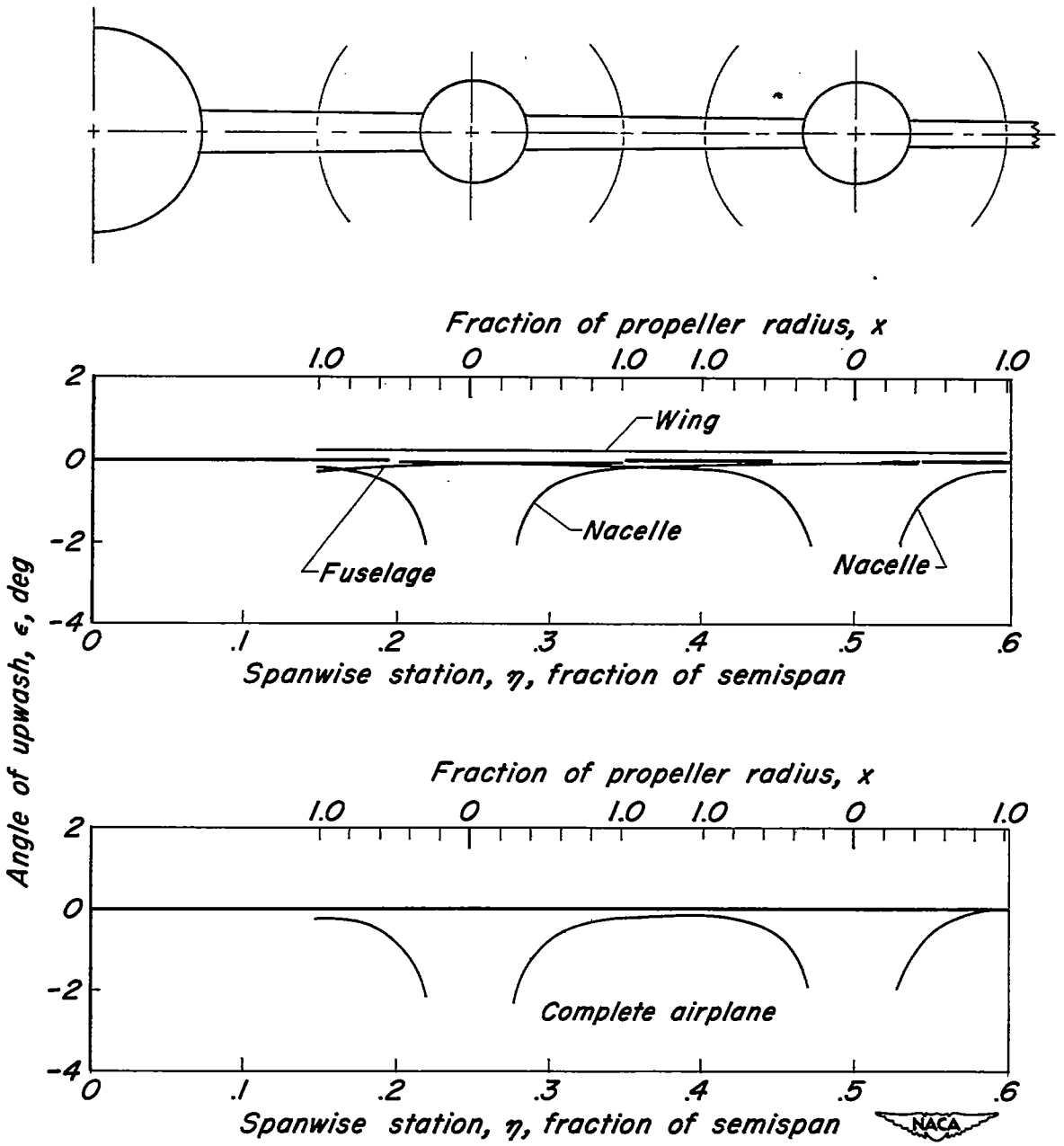

(b) Λ, 0°; a_w, 1.2°; $\gamma_{in'bd}$ -5.1°; $\gamma_{out'bd}$, -4.7°.

Figure 15.- Concluded.

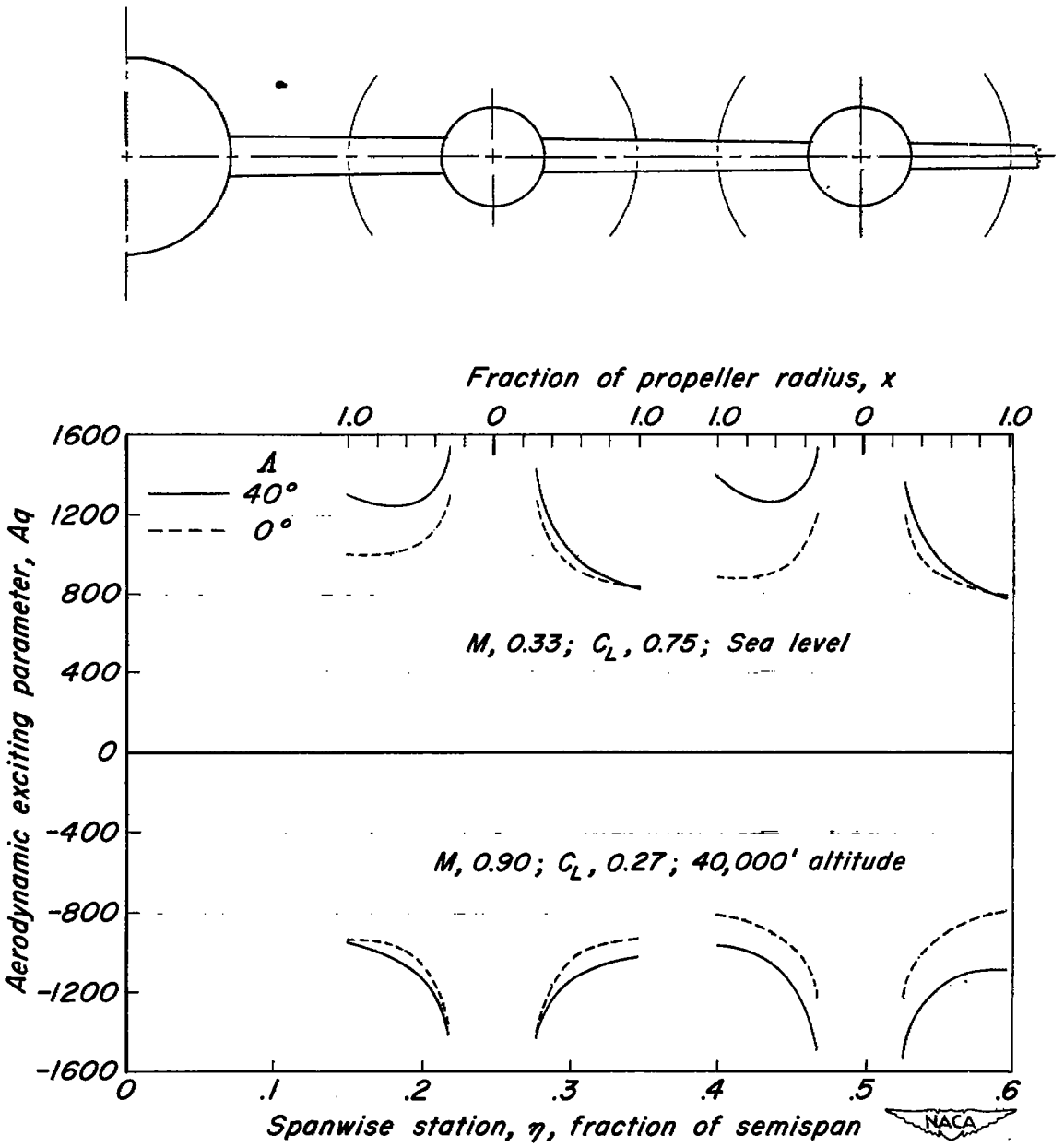

Figure 16.– The aerodynamic exciting parameter distributions at the horizontal center lines of the propeller disks of the two hypothetical airplanes with the nacelles inclined.

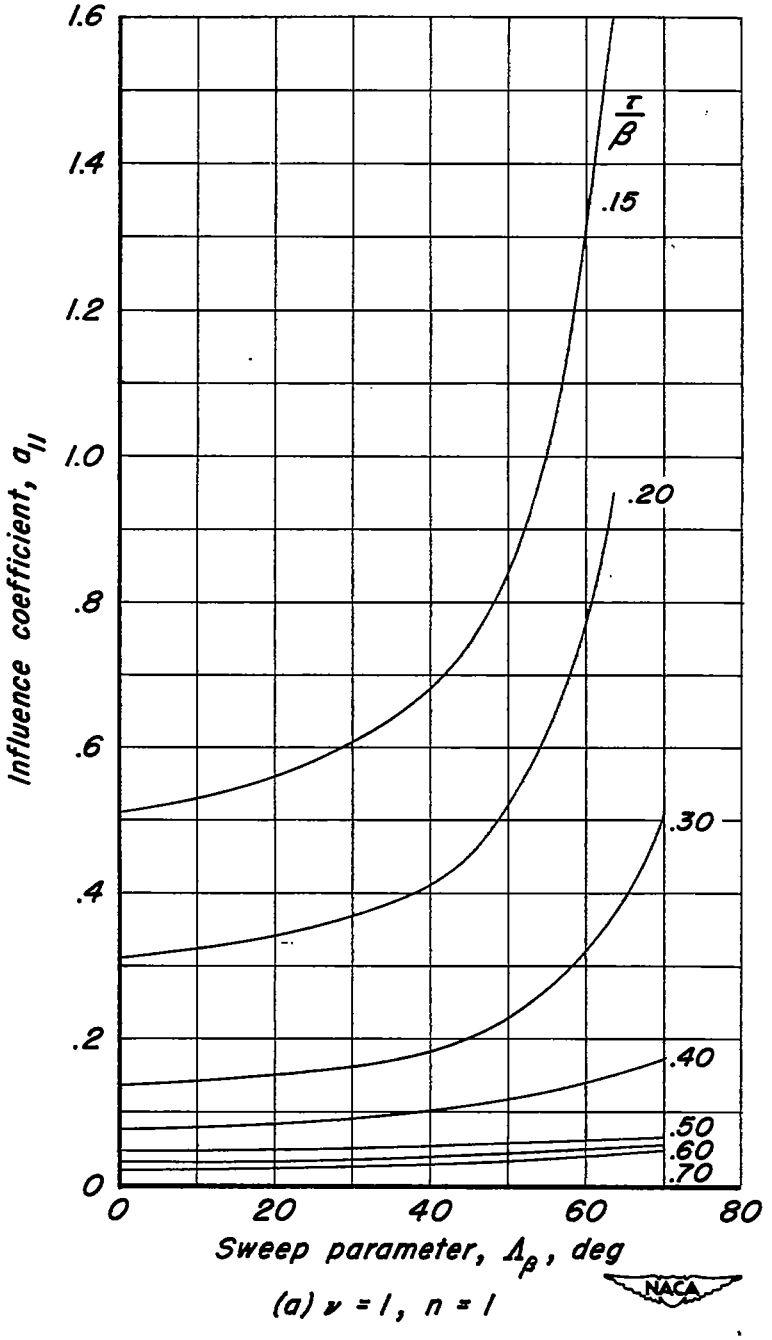

(a) $\nu = 1$, $n = 1$

Figure 17.- Influence coefficients, $a_{\nu n}$, for symmetric span loading plotted as a function of the sweep parameter, Λ_β, for various distances ahead of the wing quarter-chord line, τ/β.

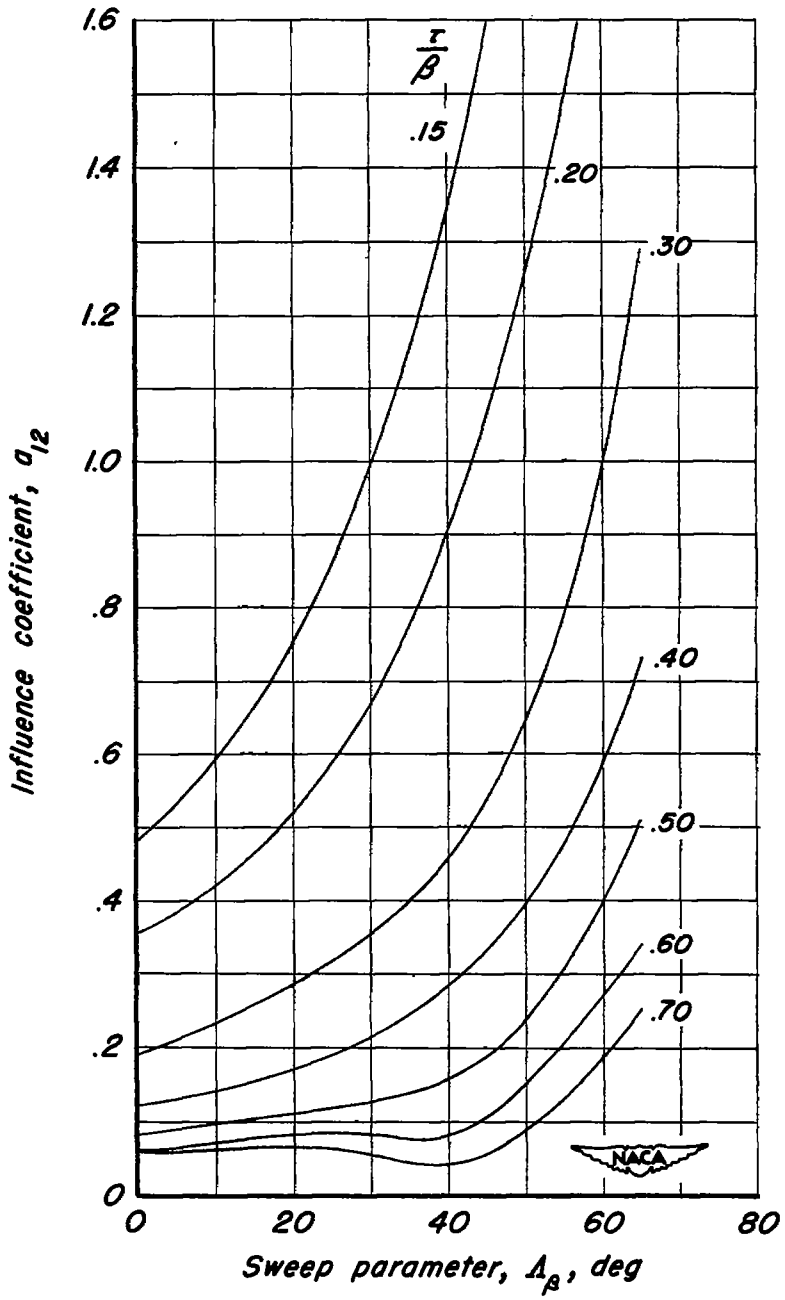

(b) $\nu = 1$, $n = 2$.

Figure 17.– Continued.

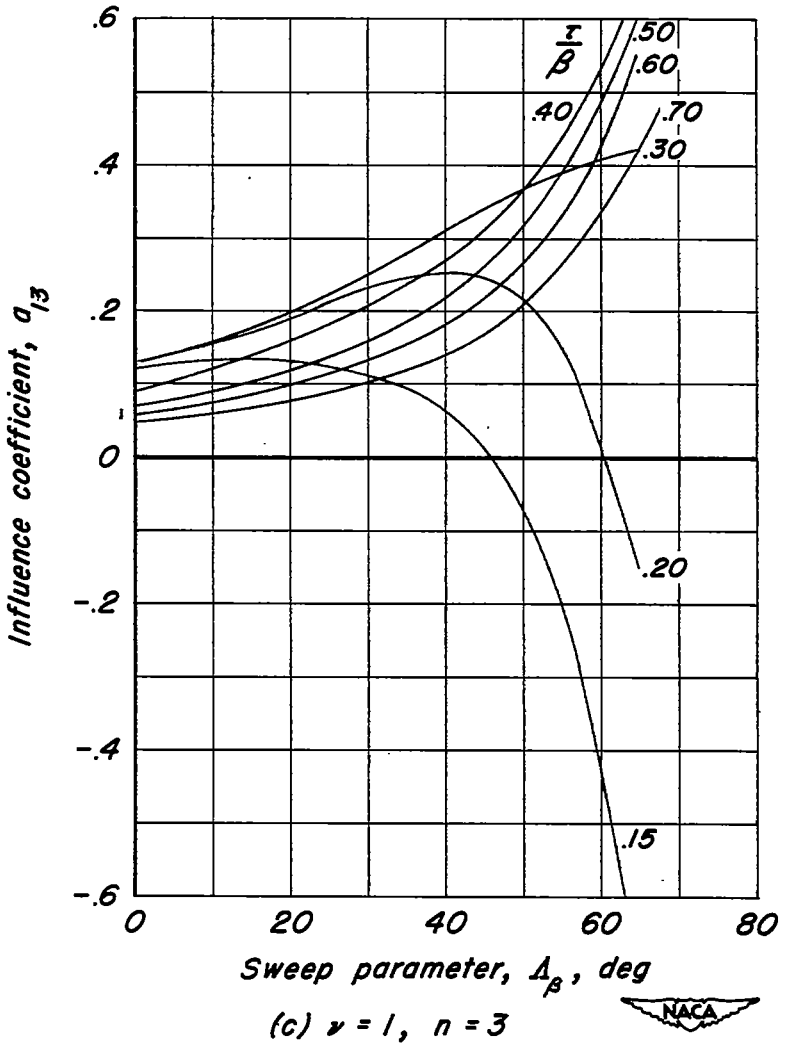

(c) $\nu = 1$, $n = 3$

Figure 17.- Continued.

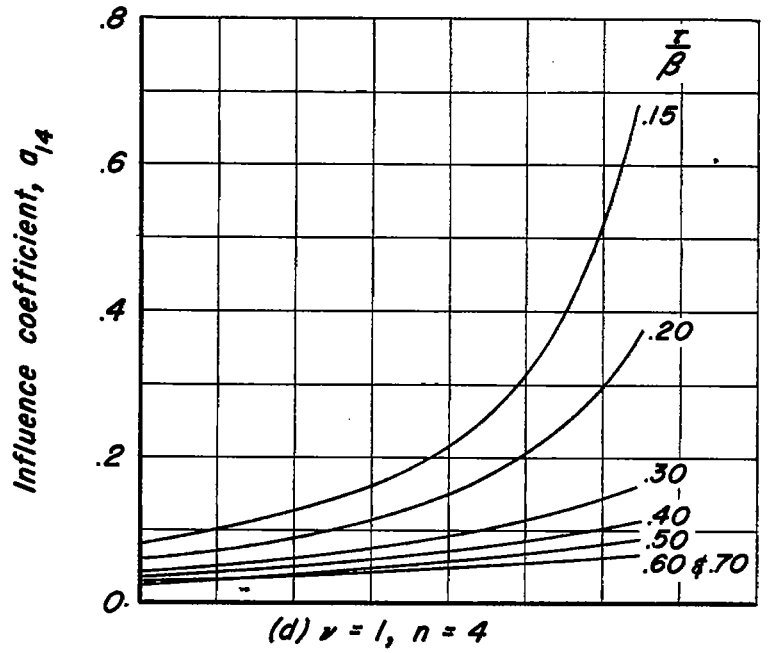

(d) $\nu = 1$, $n = 4$

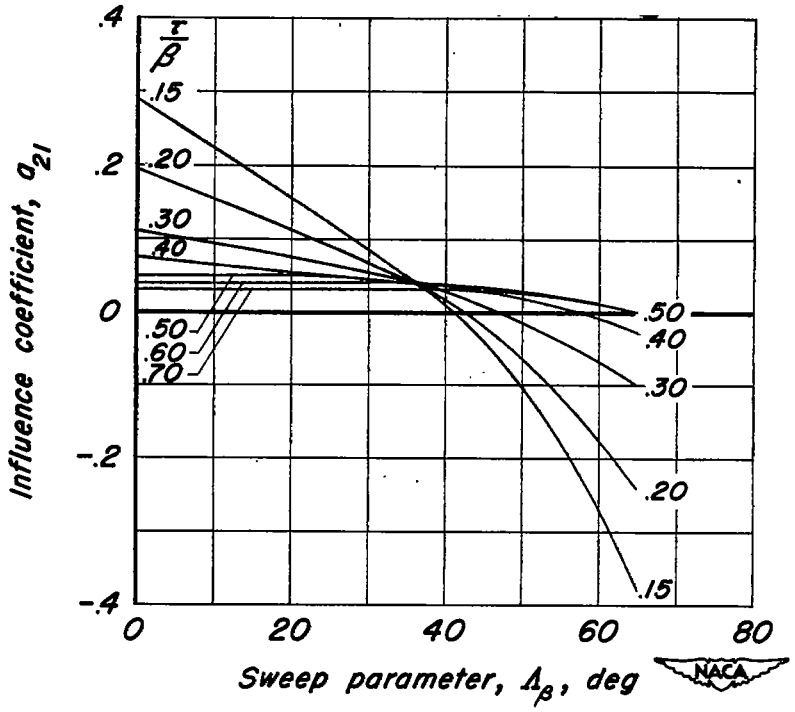

(e) $\nu = 2$, $n = 1$

Figure 17.- Continued.

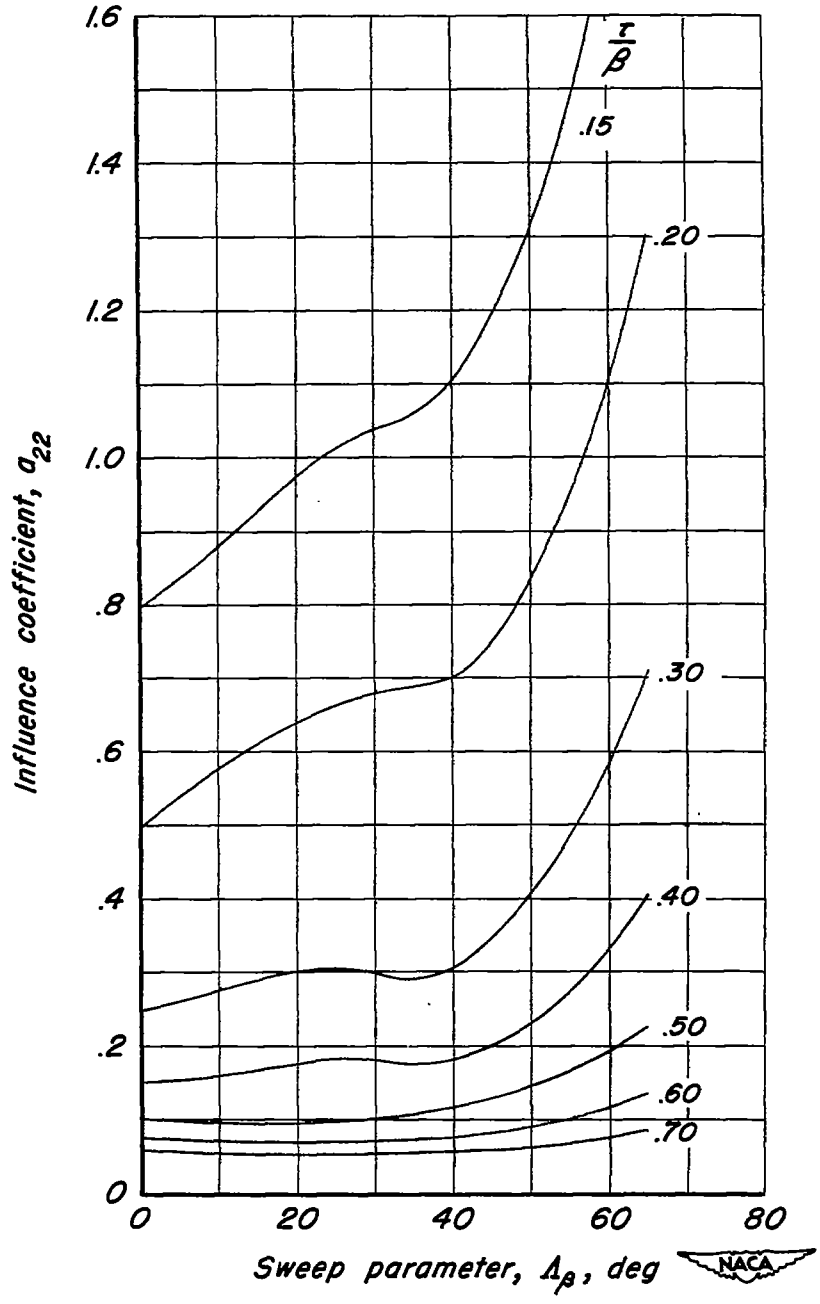

(f) $\nu = 2$, $n = 2$

Figure 17.- Continued.

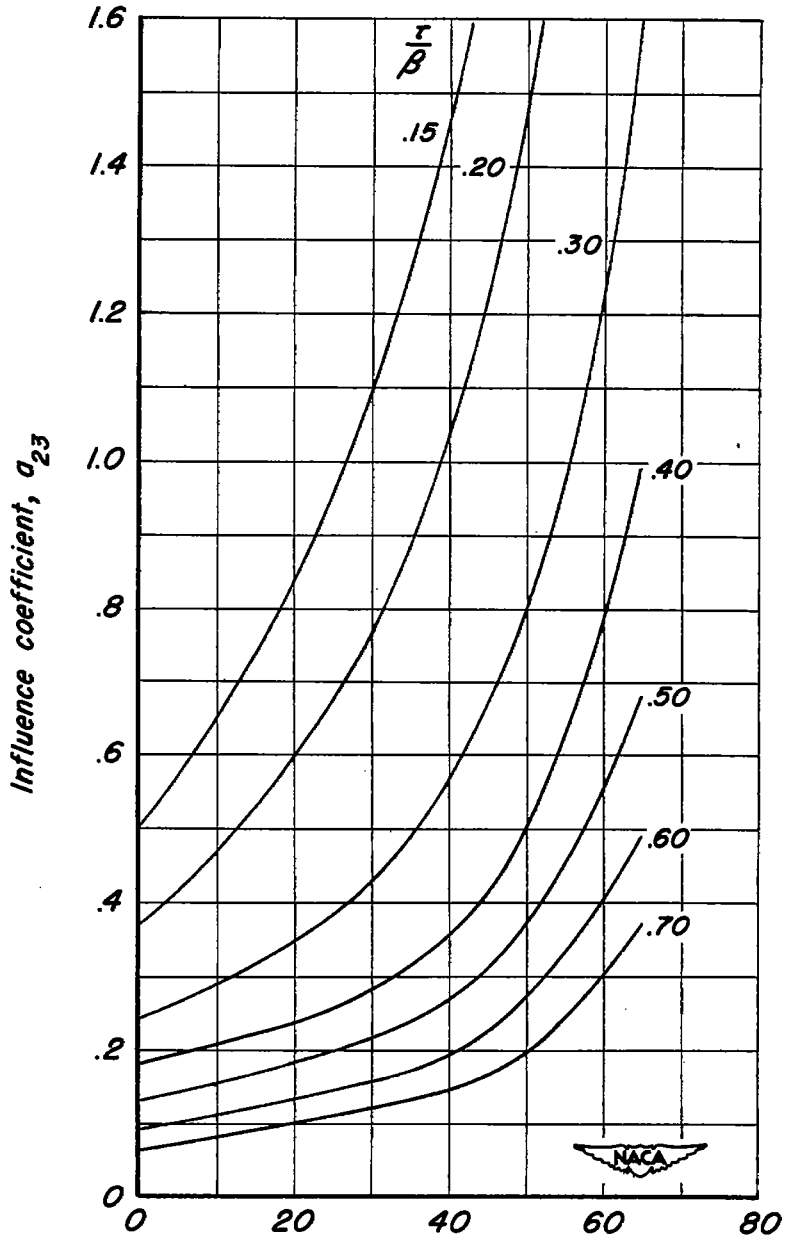

(g) $\nu = 2$, $n = 3$.

Figure 17.– Continued.

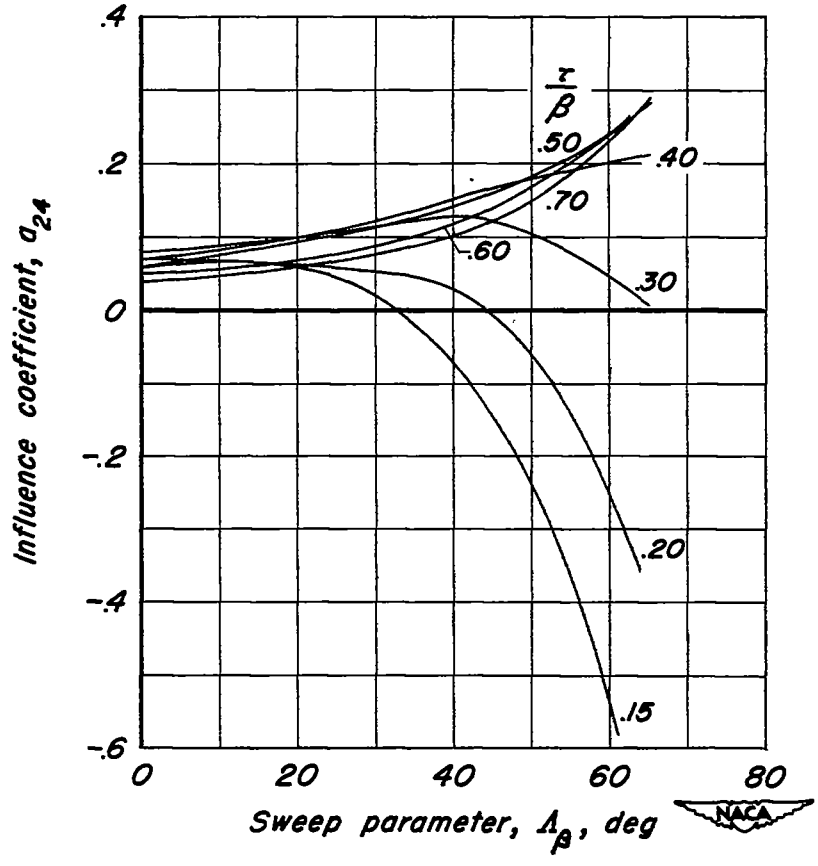

(h) $\nu = 2$, $n = 4$

Figure 17.- Continued.

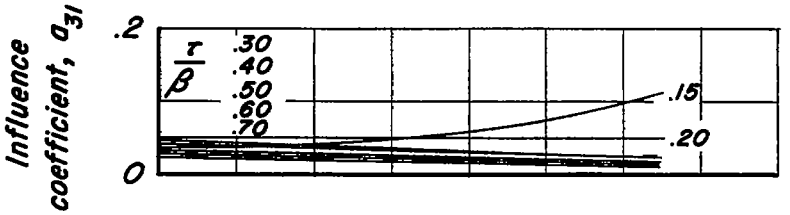

(i) $\nu = 3$, $n = 1$

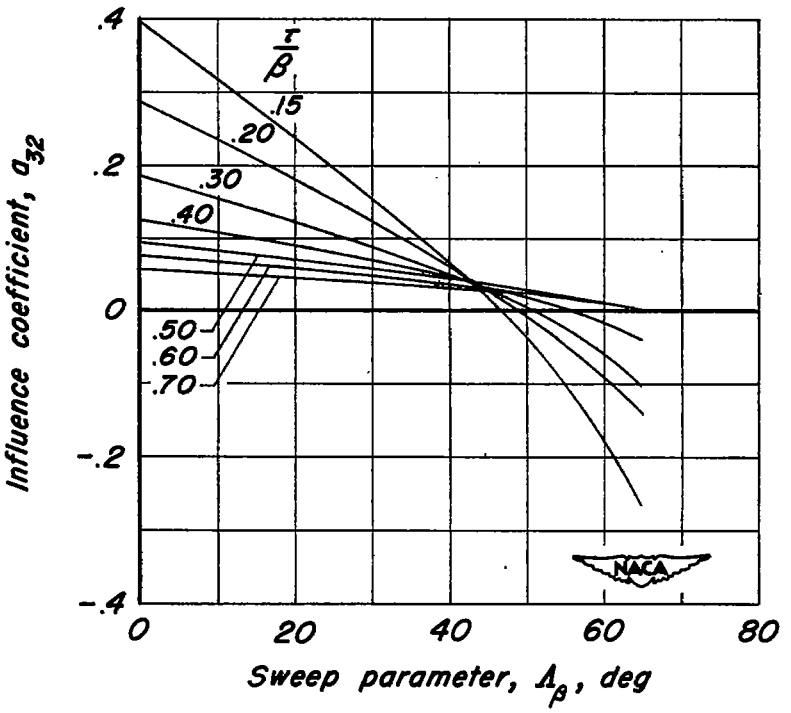

(j) $\nu = 3$, $n = 2$.

Figure 17.- Continued.

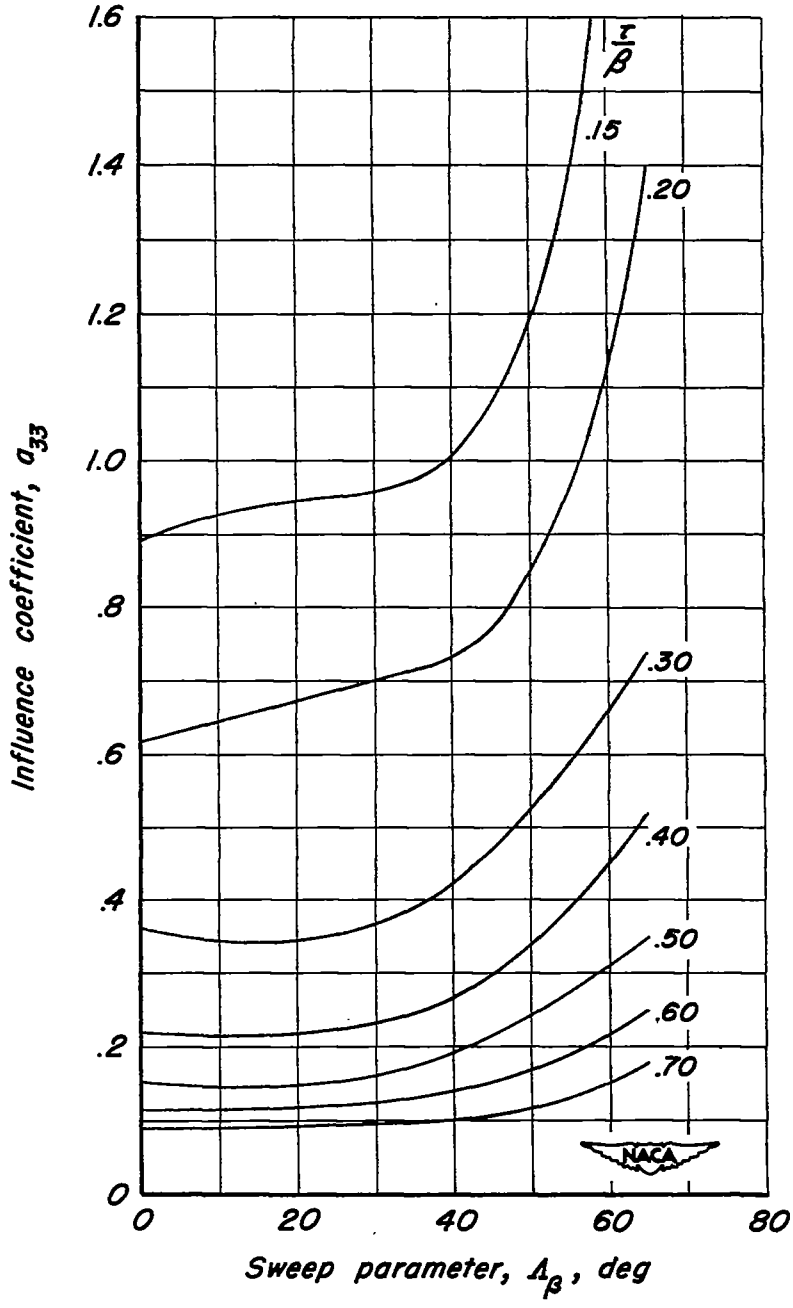

(k) $\nu = 3$, $n = 3$

Figure 17.- Continued.

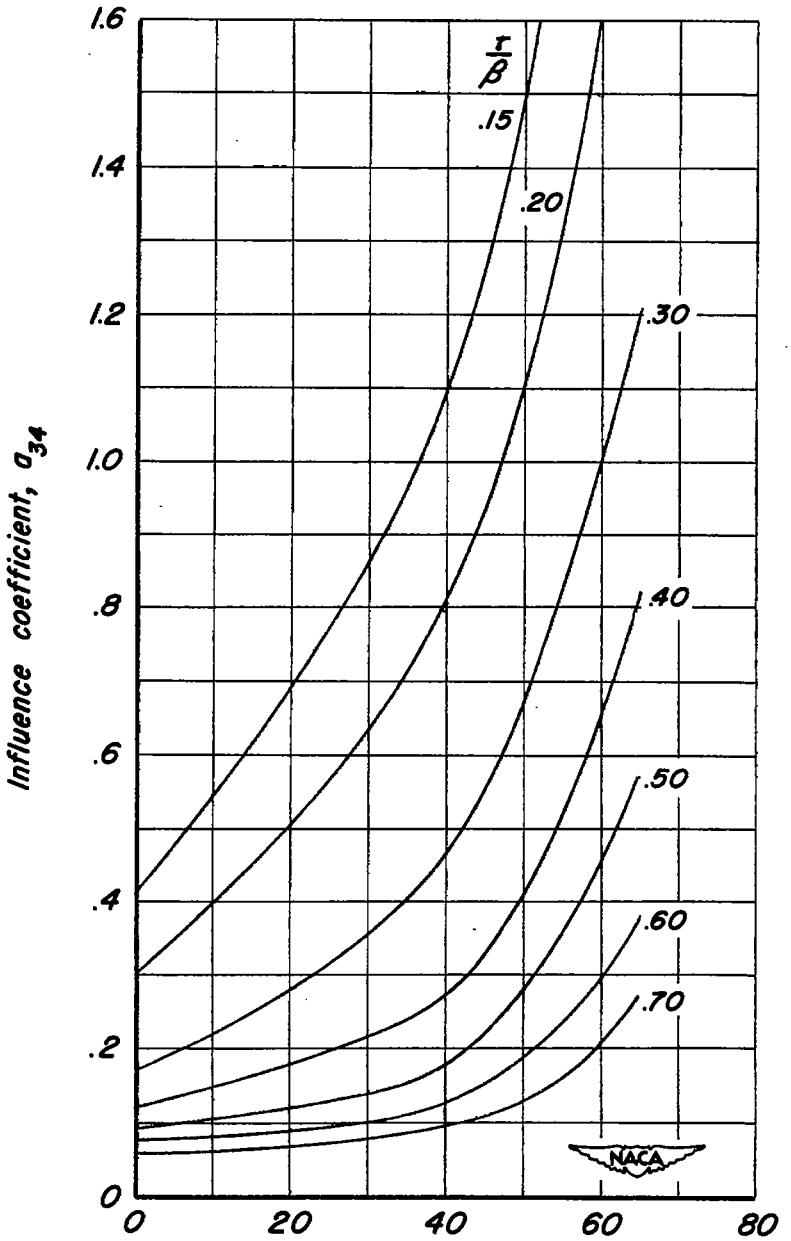

(l) $\nu = 3$, $n = 4$

Figure 17.- Continued.

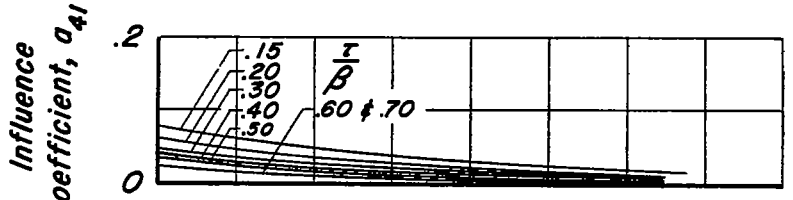

(m) $\nu = 4$, $n = 1$

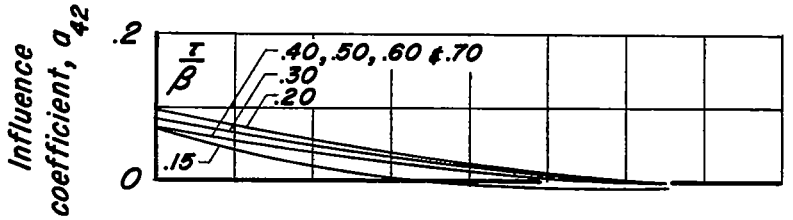

(n) $\nu = 4$, $n = 2$

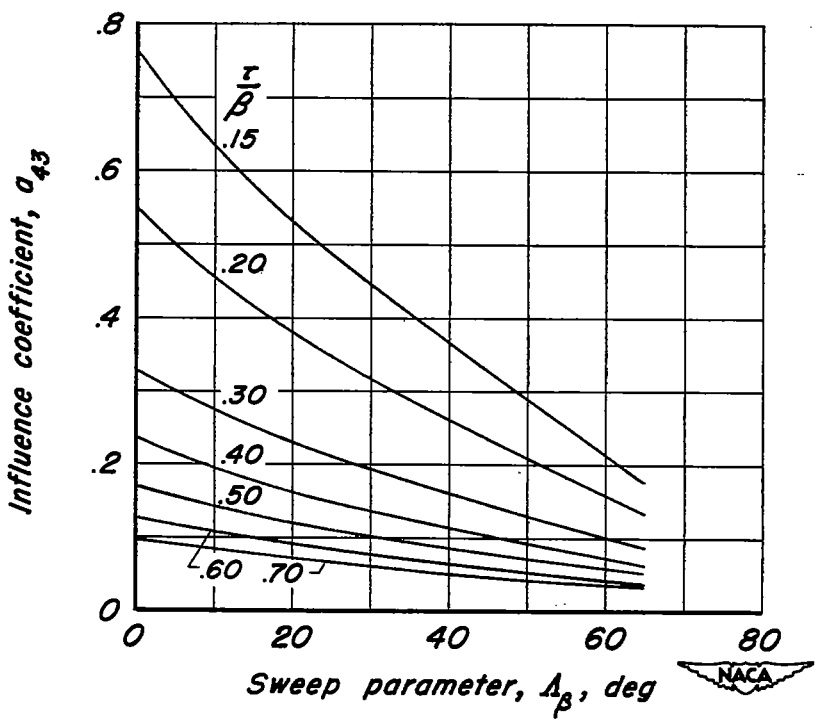

(o) $\nu = 4$, $n = 3$.

Figure 17.- Continued.

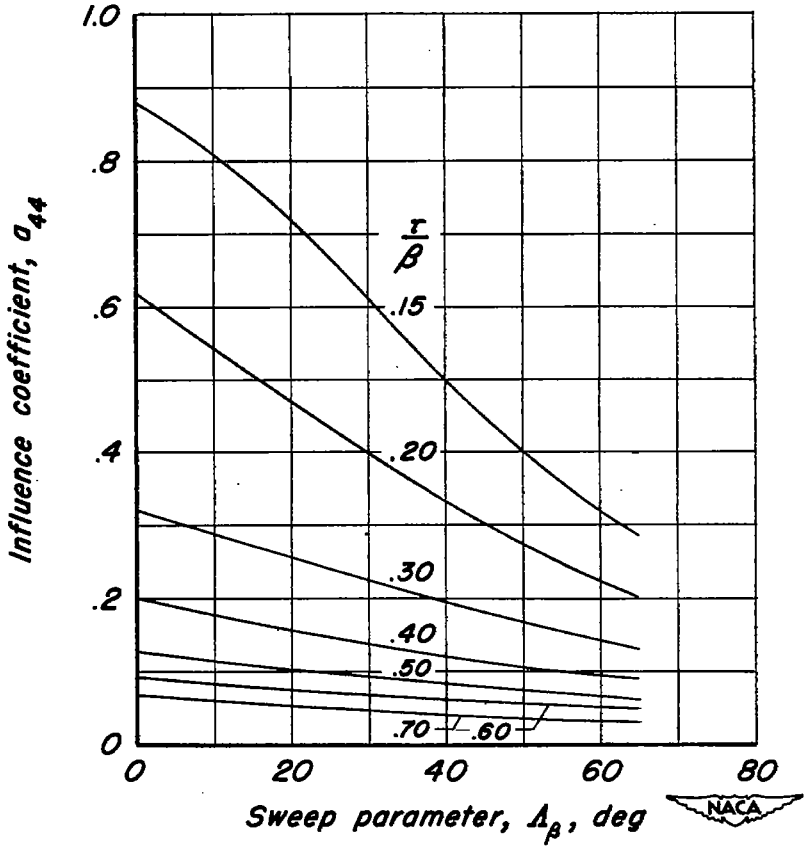

(p) $\nu = 4$, $n = 4$

Figure 17.- Concluded.